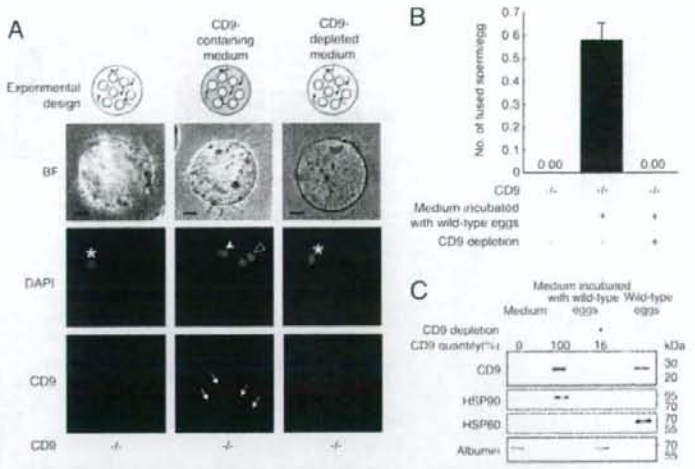

Fig. 4. Identification of fusion-facilitating activity of CD9-containing vesicles. (*A*) Estimation of the fusion-facilitating ability of the vesicles in sperm–egg fusion. As shown in the experimental design, CD9$^{-/-}$ sperm were incubated with CD9$^{+/+}$ eggs (white circles) in media containing egg-released vesicles after the zona pellucida was removed from these eggs. CD9 was detected by anti-CD9 mAb conjugated with Alexa488. The eggs were preloaded with DAPI before incubation with the sperm, to allow counting of the number of fused sperm. (*Left*) CD9$^{-/-}$ eggs at 1 h after incubation with the sperm, as a negative control. *Center* CD9$^{-/-}$ eggs cultured in the medium containing CD9 collected from wild-type eggs. (*Right*) CD9$^{-/-}$ eggs cultured in the medium depleted of CD9 by beads conjugated with anti-CD9 mAb, showing the fused sperm to eggs (arrowhead), metaphase II–arrested chromosomes (*), a second polar body (open arrowhead), and CD9 translocated on the sperm heads (arrow). The fluorescent z-series images were projected as three-dimensional images. Scale bar: 20 μm. (*B*) Number of fused sperm with the zona-free eggs counted at 1 h after incubation (mean SEM): CD9$^{-/-}$ eggs as a negative control (n 51), CD9$^{-/-}$ eggs cultured in the medium containing CD9 (n 112), and CD9$^{-/-}$ eggs cultured in the medium depleted of CD9 by antibody-conjugated beads (n 74). The total numbers of eggs examined are in parentheses. (*C*) Western blot analysis of the media incubated with CD9$^{+/+}$ eggs for CD9, HSP90, and HSP60. Loaded samples (left to right): The medium as a negative control, the medium containing the remnant material from 40 eggs per lane (bead-untreated and -treated), and 5 eggs per lane as a positive control. The albumin contained in the medium was detected by Coomassie brilliant blue staining as an internal control. The quantities of CD9 in the media were measured densitometrically (using National Institutes of Health Image software).

that the decreased amount of CD9 after the bead treatment was synchronized with that of a cytoplasmic chaperone, HSP90 (17), but not with a mitochondrial chaperone, HSP60 (18). Our analysis of the egg-conditioned medium indicated that CD9-containing vesicles contained HSP90, a conserved component of exosomes (9, 10).

To estimate the contribution of CD9-containing vesicles to sperm–egg fusion, we examined the restoration of the impaired sperm-fusing ability in CD9 eggs co-incubated with CD9 or CD9 eggs expressing endogenous CD9 (Figs. 5 and S4*A*). **We predicted that when sperm were incubated with a mixture of eggs, the vesicles released from CD9$^{+/-}$ or CD9$^{+/+}$ eggs would**

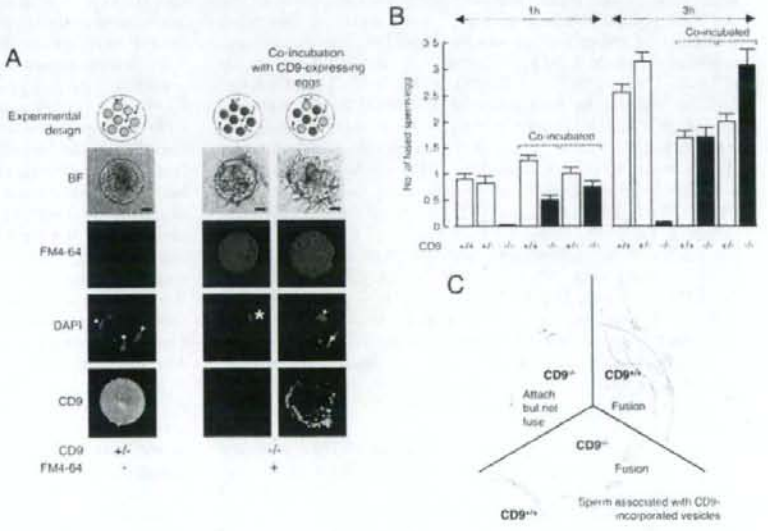

Fig. 5. Recovery of impaired fusion of CD9$^{-/-}$ eggs with sperm by CD9-containing vesicles. (*A*) Estimation of the fusion-facilitating ability of the vesicles in sperm–egg fusion. As shown in the experimental design, sperm were incubated with a mixture of CD9-expressing eggs (green circles) and CD9$^{-/-}$ eggs (red circles) after the zona pellucida was removed from these eggs. The eggs were preloaded with DAPI before incubation with sperm, to allow counting of the number of fused sperm. CD9$^{-/-}$ eggs were prestained with FM4–64 and thus were easily distinguished from CD9-expressing eggs after incubation with the sperm. (*Left*) CD9$^{-/-}$ eggs at 1 h after incubation with the sperm, as a positive control. (*Center*) CD9$^{-/-}$ eggs, as a negative control. (*Right*) CD9$^{-/-}$ eggs co-incubated with CD9$^{+/+}$ eggs, showing fused sperm to egg (arrowheads), metaphase II–arrested chromosomes (*), and extruded second polar body (arrow). The fluorescent z-series images were projected as three-dimensional images. CD9 was detected by anti-CD9 mAb conjugated with Alexa488. Scale bar: 20 μm. (*B*) Numbers of fused sperm with the zona-free eggs counted at 1 and 3 h after incubation (mean SEM). CD9$^{-/-}$ (1 h: n 34; 3 h: n 55), CD9$^{+/-}$ (1 h: n 71; 3 h: n 79), and CD9$^{-/-}$ eggs (1 h: n 100; 3 h: n 115) were separately incubated with sperm. Total number of coincubated eggs examined: CD9$^{+/+}$ eggs (n 54) coincubated with CD9$^{-/-}$ eggs (n 60), and CD9$^{+/-}$ eggs (n 65) coincubated with CD9$^{-/-}$ eggs (n 74) at 1 h; CD9$^{+/+}$ eggs (n 51) coincubated with CD9$^{-/-}$ eggs (n 33), and CD9$^{+/-}$ eggs (n 98) coincubated with CD9$^{-/-}$ eggs (n 90) at 3 h. (*C*) Schematic model of involvement of CD9-containing vesicles in sperm–egg fusion: CD9$^{+/-}$ (green), CD9$^{-/-}$ (light blue), and CD9$^{-/-}$ eggs coincubated with CD9$^{+/+}$ wild-type eggs with sperm (yellow).

interact with sperm, and these sperm could fuse with CD9 eggs. If sperm-fusing ability were regulated mainly by CD9-containing vesicles, then the number of sperm fused to CD9 eggs would be predicted to be almost equal to that fused to CD9 or CD9 eggs coincubated with CD9 eggs. We counted the number of fused sperm in coincubated CD9-expressing eggs (CD9 and CD9) and CD9 eggs. The CD9 eggs were prestained with FM4–64 (19), a fluorescent dye used to stain the membrane of live cells, and thus could be easily distinguished from the CD9 and CD9 eggs. FM4–64 did not transfer between the CD9 eggs and the CD9 or CD9 eggs. As shown in the experimental design, after the zona pellucida was removed from the eggs, CD9 eggs (red circles) were mixed with CD9 or CD9 eggs (green circles), and sperm were added to the medium containing these eggs (Fig. 5*A*). At 1 h after insemination, significant fusion of sperm with the CD9 eggs was facilitated (0.75 ± 0.11 and 0.50 ± 0.09 sperm fused per egg), corresponding to that in the CD9 (1.00 ± 0.13) and CD9 eggs (1.25 ± 0.10). At 3 h after insemination, the fusion of sperm with the CD9 eggs was restored (3.06 ± 0.30 and 1.70 ± 0.18 sperm fused per egg) to levels comparable to those in the CD9 (2.00 ± 0.15) and CD9 eggs (1.69 ± 0.13). We also detected a second polar body extruding from the CD9 eggs (Fig. 5*A Right*, arrow). In contrast, we did not observe the translocation of vesicles from the CD9 and CD9 eggs to the CD9 eggs when sperm were not added to the mixture, even after 10 h of incubation (Fig. S4*B*). These data demonstrate that the defect in the fusing ability of CD9$^{-/-}$ eggs is caused by dysfunction of the mechanism facilitating the sperm-fusing activity through CD9-containing vesicles.

To further study the involvement of CD9-containing vesicles in regulating sperm-fusing ability, we evaluated the capability of hamster eggs in sperm–egg fusion (Fig. S5). Hamster eggs have the ability to fuse with other mammalian sperm and thus are used as a tool to evaluate the fusing ability of human sperm (20). When hamster eggs were incubated with CD9$^{-/-}$ eggs after the zona pellucida was removed from these eggs, the sperm-fusing ability of these eggs was improved significantly. The sperm-fusing ability acquired through the exposure to hamster eggs was not as great as that produced by exposure to mouse eggs, probably due to the slightly different CD9 in hamster and mouse eggs (21). These results indicate that the function of CD9-containing vesicles in the acquisition of sperm-fusing ability is widely conserved in mammals.

Discussion

In sperm–egg fusion, there is a significant direct interaction between the cell membranes of sperm and eggs (1, 20, 22); however, our results demonstrate that CD9-containing vesicle–sperm interaction precedes the direct cell membrane interaction between sperm and eggs. Based on our data, we propose that the release of CD9-containing vesicles from eggs before fertilization facilitates the sperm-fusing ability that renders the sperm competent to fuse with CD9$^{-/-}$ eggs (Fig. 5*C*). Our finding of CD9-EGFP in living unfertilized eggs demonstrates that CD9-containing vesicles are present in the PVS, and that these vesicles accumulate inside the PVS during the germinal vesicle (1) and metaphase II-arrested stages (1). During this period, the egg undergoes drastic cytological changes with the increased number of microvilli (1, 22), predicting the correlation between vesicle release and microvilli formation. As expected, this correlation is supported by the finding that CD9 deficiency leads not only to impaired microvilli formation (8) (Fig. S2), but also to decreased accumulation of vesicles within the PVS. These data support the association between the release of CD9-containing vesicles from eggs and the formation of microvilli on the egg plasma membrane.

As reported previously, somatic cells are capable of releasing proteins and lipids included in membrane organelles, termed exosomes (9, 10), which are pinched out from the plasma membrane (23). Exosomes share many additional properties with retroviral particles, including similar lipid and protein compositions, such as tetraspanin (23). GM3 and HSP90 are known to be conserved components of exosomes (10). Our results show that CD9-containing vesicles released from eggs share these two components, implying that the vesicles are "exosome-like." Previous studies of macrophages have proposed that exosome biogenesis occurs only by outward budding at endosomal membranes, followed by the fusion of vesicle-laden endosomes with the plasma membrane (9, 23). If the CD9-containing vesicle were derived from exosomes and generated from the fusion of endosomes with the plasma membrane, then the vesicles would contain some proteases (9, 23), fuse with the sperm membrane, and possibly activate the sperm fusogenic factor(s) by enzymatic activities.

In hamster eggs, expansion of the PVS has been deemed essential or at least beneficial to normal fertilization (20, 21, 24), indicating that materials involved in fusion with sperm are released from eggs before fertilization in hamsters and in mice. Because anti-CD9 mAbs are not available for hamster CD9, we could not directly confirm CD9-containing vesicle release from hamster eggs before fertilization. Instead, our co-incubation assay demonstrated that hamster eggs facilitate the fusion of sperm with CD9$^{-/-}$ eggs, indicating that hamster eggs share a similar mechanism with mouse eggs through egg-released materials. Moreover, it has been reported that growing oocytes bind to sperm and transfer fluorescent dyes to the sperm head (25). At this stage, oocytes have CD9 on the cell membrane but lack CD9-containing vesicles (Fig. S1). We presume that the transfer of fluorescent dye from growing oocytes to sperm heads is mediated by CD9 on the cell membrane. Based on our findings, we propose that the CD9-containing vesicle has an ability to facilitate sperm—egg fusion. This knowledge has great potential for clinical applications, such as the induction of sperm–egg fusion using exogenous sources.

Materials and Methods

Animals. The mice that we produced were back-crossed into a C57BL/6 genetic background. Wild-type eggs were collected from C57BL/6 females (8–12 weeks old). Wild-type sperm were obtained from the epididymides of B6C3F1 males (8–12 weeks old). Hamster eggs were obtained commercially as frozen unfertilized eggs (NOSAN).

Antibodies and Chemicals. Antibodies against CD9 (KMC; BD PharMingen), beta-tubulin (Tub2.1; Sigma), HSP60 (24/HSP60; BD PharMingen), HSP90 (16F1; MBL), and GM3 (GMR6; Seikagaku) were used. Antibodies labeled with biotin by a labeling kit (Dojindo) and horseradish peroxidase-conjugated streptavidin (Sigma) were used for Western blot analysis. For immunostaining, antibodies were labeled directly with Alexa488 and Alexa546 using labeling kits (Invitrogen). FM4–64 (Invitrogen) was used to define the lipid bilayer of live eggs without disturbing sperm–egg fusion (10 μM at final concentration). We used DAPI (Invitrogen), a fluorescent dye that slowly permeates the living cell membrane (semipermeable) and slowly leaks out of cells after washing relative to Hoechst33342 (permeable), in counting the number of sperm fused per egg.

Transgenic Mice. The construct expressing mouse CD9 tagged at the N terminus with EGFP (CD9-EGFP) was subcloned into plasmid DNA-containing mouse ZP3 promoter (26). The expression cassette was excised by restriction enzyme digestion and microinjected into fertilized eggs of C57BL/6 mice, according to standard techniques (27).

Genotyping and RT-PCR. Mouse genotyping and RT-PCR were performed following standard procedures (27). (Primer sets are listed in Table S1).

Egg Collection. Eggs were collected from the oviduct 14–16 h after human chorionic gonadotropin injection (4). The eggs were placed in a drop of TYH

medium (28). Sperm collected from the epididymides were capacitated in a 100-μl drop of medium. The eggs were incubated with 1.5 × 10^5 sperm/ml at 37°C in 5% CO_2, and unbound sperm were washed away. The zona pellucida was removed from the eggs with acidic Tyrode's solution (4) or a piezo manipulator (11). A hole was punched through the zona pellucida with a piezo manipulator, and the eggs were removed. All materials were aspirated, including the medium but not the eggs, and used as "remnants."

Immunostaining. Zona-intact live eggs were stained with diluted antibodies in TYH medium for 30 min at 37°C, and the nonspecifically accumulated antibodies in the PVS were washed away after a brief incubation (30 min) in the medium. To measure the fluorescent intensities of GM3, three types of eggs were stained by Alexa546-labeled anti-GM3 mAb in TYH medium for 30 min, then washed in the medium for 30 min. Staining was visualized using a laser scanning confocal microscope (LSM 510 META; Carl Zeiss).

Electron-Microscopic Analysis. Live eggs were incubated with anti-CD9 mAb and anti-rat IgG mAb tagged with 5-nm gold beads. After incubation, the eggs were fixed by glutaraldehyde and osmic acid solutions. Ultra-thin sections were prepared as described in ref. 29. Eggs denuded with acid Tyrode's solution were fixed with a mixture of paraformaldehyde and glutaraldehyde and osmic acid solutions.

***In Vitro* Fertilization.** To observe the fusion with the sperm, zona-intact and zona-free eggs were incubated with DAPI (10 μg/ml) in the medium for 20 min, then washed before the sperm were added. This procedure allowed the staining of only fused sperm nuclei by dye-transfer into sperm after membrane fusion. At 1 h or 3 h after incubation in a 30-μl drop of medium, the eggs were fixed with a mixture of paraformaldehyde and glutaraldehyde for 20 min at 4°C.

Monitoring the Association of CD9-Containing Vesicles with Sperm. Eggs collected from Tg$^-$CD9$^{-/-}$ females were set in a 30-μl drop of TYM medium. The sperm were added to the eggs at a final concentration of 1.5 × 10^5/ml after incubation in the medium for 2 h. Posts of latex beads were deposited around the eggs. A glass coverslip was carefully pressed down onto the posts until the egg were fixed. The medium containing eggs and sperm was cooled to 10°C before observation. Cooling reduced the sperm motility. This procedure allowed us to measure the CD9-EGFP fluorescence on the sperm head using a confocal microscope. Images of the sperm were captured at 1 frame/s. The average value of the fluorescent intensities of CD9-EGFP at 0 s was set to 100%, and the final concentration of antibodies was adjusted to 50 μg/ml. The data are measurements of serial images from 15 wild-type sperm in triplicate dishes.

Collection of CD9-Containing Vesicles. The medium containing the vesicles was collected from denuded wild-type eggs. The eggs were cultured in a 60-μl drop of medium for 2 h after the zona pellucida was removed from the eggs. Collecting the medium containing the vesicles required an incubation time of 2 h. The collected medium was used for analysis of vesicle components and evaluation of sperm-fusing ability. CD9-depleted medium was used as a negative control. After the zona pellucida was removed from CD9$^{-/-}$ eggs, the eggs were incubated with the sperm in the medium containing CD9-incorporated vesicles for 1 h, for comparison with the vesicle-depleted medium. Details are shown in Fig. S3.

Western Blot Analysis. Quantities of proteins were examined by Western blot analysis, as described in ref. 4. As an internal loading control, quantities of albumin included in the medium were examined using Coomassie brilliant blue staining. Details are shown in Fig. S3.

Coincubation of Two Types of Eggs. CD9$^{-/-}$ eggs and CD9-expressing eggs (CD9$^{+/-}$ and CD9$^{+/+}$) were incubated in each 30-μl drop of medium after the zona pellucida was removed from these eggs. At 2 h after incubation, the CD9$^{-/-}$ eggs were added into the cultured medium of the CD9-expressing eggs. Sperm were added into the medium containing two types of eggs and incubated for 1 or 3 h. Details are shown in Fig. S4A. The frozen hamster eggs also were incubated with the CD9$^{-/-}$ eggs and wild-type sperm for 1 h. The zona pellucida of frozen hamster eggs was hardened, and removing the zona pellucida using acid Tyrode's solution took 5 min. Details are shown in Fig. S5A.

ACKNOWLEDGMENTS. This work was supported by a Precursory Research for Embryonic Science and Technology (PRESTO) grant from the Japanese Ministry of Health, Labor and Welfare and by a Grant-in-Aid for Scientific Research from the Japanese Ministry of Education, Culture, Sports, and Technology.

1. Yanagimachi R (1994) in *The Physiology of Reproduction*, eds Knobil E, Neill JD (Raven, New York), pp 189–317.
2. Kaji K, *et al.* (2000) The gamete fusion process is defective in eggs of Cd9-deficient mice. *Nat Genet* 24:279–282.
3. Le Naour F, Rubinstein E, Jasmin C, Prenant M, Boucheix C (2000) Severely reduced female fertility in CD9-deficient mice. *Science* 287:319–321.
4. Miyado K, *et al.* (2000) Requirement of CD9 on the egg plasma membrane for fertilization. *Science* 287:321–324.
5. Hemler ME (2003) Tetraspanin proteins mediate cellular penetration, invasion, and fusion events and define a novel type of membrane microdomain. *Annu Rev Cell Dev Biol* 19:397–422.
6. Barraud-Lange V, Naud-Barriant N, Bomsel M, Wolf J-P, Ziyyat A (2007) Transfer of oocyte membrane fragments to fertilizing spermatozoa. *FASEB J* 21:3446–3449.
7. Joly E, Hudrisier D (2003) What is trogocytosis and what is its purpose? *Nat Immunol* 4:815.
8. Runge K-E, *et al.* (2007) Oocyte CD9 is enriched on the microvillar membrane and required for normal microvillar shape and distribution. *Dev Biol* 304:317–325.
9. Trajkovic K, *et al.* (2008) Ceramide triggers budding of exosome vesicles into multivesicular endosomes. *Science* 319:1244–1247.
10. Wubbolts R, *et al.* (2003) Proteomic and biochemical analyses of human B cell-derived exosomes: Potential implications for their function and multivesicular body formation. *J Biol Chem* 278:10963–10972.
11. Yamagata K, *et al.* (2002) Sperm from the calmegin-deficient mouse have normal abilities for binding and fusion to the egg plasma membrane. *Dev Biol* 250:348–357.
12. Mitsuzuka K, Handa K, Satoh M, Arai Y, Hakomori S (2005) A specific microdomain ("glycosynapse 3") controls phenotypic conversion and reversion of bladder cancer cells through GM3-mediated interaction of alpha3beta1 integrin with CD9. *J Biol Chem* 280:35545–35553.
13. Yamashita T, *et al.* (2003) Enhanced insulin sensitivity in mice lacking ganglioside GM3. *Proc Natl Acad Sci USA* 100:3445–3449.
14. Kotani M, Ozawa H, Kawashima I, Ando S, Tai T (1992) Generation of one set of monoclonal antibodies specific for a-pathway ganglio-series gangliosides. *Biochim Biophys Acta* 1117:97–103.
15. Chen MS, *et al.* (1999) Role of the integrin-associated protein CD9 in binding between sperm ADAM 2 and the egg integrin alpha6beta1: Implications for murine fertilization. *Proc Natl Acad Sci USA* 96:11830–11835.
16. Miller B-J, Georges-Labouesse E, Primakoff P, Myles D-G (2000) Normal fertilization occurs with eggs lacking the integrin alpha6beta1 and is CD9-dependent. *J Cell Biol* 149:1289–1296.
17. Callahan M-K, Garg M, Srivastava P-K (2008) Heat-shock protein 90 associates with N-terminal extended peptides and is required for direct and indirect antigen presentation. *Proc Natl Acad Sci USA* 105:1662–1667.
18. Cheng M-Y, Hartl F-U, Horwich A-L (1990) The mitochondrial chaperonin hsp60 is required for its own assembly. *Nature* 348:455–458.
19. Bolte S, *et al.* (2004) FM-dyes as experimental probes for dissecting vesicle trafficking in living plant cells. *J Microsc* 214:159–173.
20. Yanagimachi R, Yanagimachi H, Rogers B-J (1976) The use of zona-free animal ova as a test system for the assessment of the fertilizing capacity of human spermatozoa. *Biol Reprod* 15:471–476.
21. Ponce R-H, Yanagimachi R, Urch U-A, Yamagata T, Ito M (1993) Retention of hamster oolemma fusibility with spermatozoa after various enzyme treatments: A search for the molecules involved in sperm–egg fusion. *Zygote* 1:163–171.
22. Primakoff P, Myles D-G (2002) Penetration, adhesion, and fusion in mammalian sperm–egg interaction. *Science* 296:2183–2185.
23. Booth A-M, *et al.* (2006) Exosomes and HIV Gag bud from endosome-like domains of the T cell plasma membrane. *J Cell Biol* 172:923–935.
24. Okada A, Yanagimachi R, Yanagimachi H (1986) Development of a cortical granule-free area of cortex and the perivitelline space in the hamster oocyte during maturation and following ovulation. *J Submicrosc Cytol* 18:233–247.
25. Zuccotti M, Yanagimachi R, Yanagimachi H (1991) The ability of hamster oolemma to fuse with spermatozoa: Its acquisition during oogenesis and loss after fertilization. *Development* 112:143–152.
26. Rankin T-L, *et al.* (1998) Human ZP3 restores fertility in Zp3 null mice without affecting order-specific sperm binding. *Development* 125:2415–2424.
27. Hogan B, Costantini F, Lacy E (1986) in *Manipulating the Mouse Embryo* (Cold Spring Harbor Lab Press, Cold Spring Harbor, NY), pp 217–252.
28. Toyoda Y, Chang M-C (1974) Capacitation of epididymal spermatozoa in a medium with high K-Na ratio and cyclic AMP for the fertilization of rat eggs in vitro. *J Reprod Fertil* 36:125–134.
29. Toshimori K, Saxena D-K, Tanii I, Yoshinaga K (1998) An MN9 antigenic molecule, equatorin, is required for successful sperm–oocyte fusion in mice. *Biol Reprod* 59:22–29.

doi:10.1038/nature07027

LETTERS

IGFBP-4 is an inhibitor of canonical Wnt signalling required for cardiogenesis

Weidong Zhu[1]*, Ichiro Shiojima[1]*, Yuzuru Ito[2]*, Zhi Li[1], Hiroyuki Ikeda[1], Masashi Yoshida[1], Atsuhiko T. Naito[1], Jun-ichiro Nishi[1], Hiroo Ueno[3], Akihiro Umezawa[4], Tohru Minamino[1], Toshio Nagai[1], Akira Kikuchi[5], Makoto Asashima[2,6,7] & Issei Komuro[1]

Insulin-like growth-factor-binding proteins (IGFBPs) bind to and modulate the actions of insulin-like growth factors (IGFs)[1]. Although some of the actions of IGFBPs have been reported to be independent of IGFs, the precise mechanisms of IGF-independent actions of IGFBPs are largely unknown[1,2]. Here we report a previously unknown function for IGFBP-4 as a cardiogenic growth factor. IGFBP-4 enhanced cardiomyocyte differentiation *in vitro*, and knockdown of *Igfbp4* attenuated cardiomyogenesis both *in vitro* and *in vivo*. The cardiogenic effect of IGFBP-4 was independent of its IGF-binding activity but was mediated by the inhibitory effect on canonical Wnt signalling. IGFBP-4 physically interacted with a Wnt receptor, Frizzled 8 (Frz8), and a Wnt co-receptor, low-density lipoprotein receptor-related protein 6 (LRP6), and inhibited the binding of Wnt3A to Frz8 and LRP6. Although IGF-independent, the cardiogenic effect of IGFBP-4 was attenuated by IGFs through IGFBP-4 sequestration. IGFBP-4 is therefore an inhibitor of the canonical Wnt signalling required for cardiogenesis and provides a molecular link between IGF signalling and Wnt signalling.

The heart is the first organ to form during embryogenesis, and abnormalities in this process result in congenital heart diseases, the most common cause of birth defects in humans[3]. Molecules that mediate cardiogenesis are of particular interest because of their potential use for cardiac regeneration[4,5]. Previous studies have shown that soluble growth factors such as bone morphogenetic proteins (BMPs), fibroblast growth factors (FGFs), Wnts and Wnt inhibitors mediate the tissue interactions that are crucial for cardiomyocyte specification[3,4]. We proposed that there might be additional soluble factors that modulate cardiac development and/or cardiomyocyte differentiation.

P19CL6 cells differentiate into cardiomyocytes with high efficiency in the presence of 1% dimethylsulphoxide (DMSO)[6]. We cultured P19CL6 cells with culture media conditioned by various cell types in the absence of DMSO, and screened the cardiogenic activity of the conditioned media. The extent of cardiomyocyte differentiation was assessed by the immunostaining with MF20 monoclonal antibody that recognizes sarcomeric myosin heavy chain (MHC). Among the several cell types tested, culture media conditioned by a murine stromal cell line OP9 induced cardiomyocyte differentiation of P19CL6 cells without DMSO treatment (Fig. 1a, left and middle panels). Increased MF20-positive area was accompanied by the induction of cardiac marker genes such as *αMHC*, *Nkx2.5* and *GATA-4*, and by the increased protein levels of cardiac troponin T (cTnT) (Fig. 1a, right panel). In contrast, culture media conditioned by COS7 cells, mouse embryonic fibroblasts, NIH3T3 cells, HeLa cells, END2 cells (visceral endoderm-like cells), neonatal rat cardiomyocytes and neonatal rat cardiac fibroblasts did not induce cardiomyocyte differentiation of P19CL6 cells in the absence of DMSO (Fig. 1a and data not shown). From these observations, we postulated that OP9 cells secrete one or more cardiogenic growth factors.

To identify an OP9-derived cardiogenic factor, complementary DNA clones isolated by a signal sequence trap method from an OP9 cell cDNA library[7] were tested for their cardiogenic activities by transient transfection. When available, recombinant proteins were also used to confirm the results. Among candidate factors tested, IGFBP-4 induced cardiomyocyte differentiation of P19CL6 cells, as demonstrated by the increase in MF20-positive area and the induction of cardiac markers (Fig. 1b). We also cultured P19CL6 cells with OP9-conditioned media pretreated with an anti-IGFBP-4 neutralizing antibody. The application of an anti-IGFBP-4 neutralizing antibody attenuated the efficiency of cardiomyocyte differentiation induced by OP9-conditioned media (Fig. 1c). These findings strongly suggest that IGFBP-4 is a cardiogenic factor secreted from OP9 cells.

Because IGFBPs have been characterized as molecules that bind to and modulate the actions of IGFs, we tested whether IGFBP-4 promotes cardiogenesis by either enhancing or inhibiting the actions of IGFs. We first treated P19CL6 cells with a combination of anti-IGF-I and IGF-II-neutralizing antibodies or a neutralizing antibody against type-I IGF receptor. If IGFBP-4 induces cardiomyocyte differentiation by inhibiting IGF signalling, treatment with these antibodies should induce cardiomyocyte differentiation and/or enhance the cardiogenic effects of IGFBP-4. In contrast, if IGFBP-4 promotes cardiogenesis by enhancing IGF signalling, treatment with these antibodies should attenuate IGFBP-4-mediated cardiogenesis. However, treatment with these antibodies did not affect the efficiency of IGFBP-4-induced cardiomyocyte differentiation (Fig. 1d and data not shown). Treatment of P19CL6 cells with IGF-I and IGF-II also did not induce cardiomyocyte differentiation (data not shown). Furthermore, treatment with an IGFBP-4 mutant (IGFBP-4-H74P; His 74 replaced by Pro)[8] that is unable to bind IGFs induced cardiomyocyte differentiation of P19CL6 cells even more efficiently than wild-type IGFBP-4 (Fig. 1e). This is presumably due to the sequestration of wild-type IGFBP-4 but not mutant IGFBP-4-H74P by endogenous IGFs. In agreement with this idea, exogenous IGFs attenuated wild-type IGFBP-4-induced but not IGFBP-4-H74P-induced cardiogenesis (Fig. 1f). Taken together, these observations indicate

[1]Department of Cardiovascular Science and Medicine, Chiba University Graduate School of Medicine, Chiba 260-8670, Japan. [2]ICORP Organ Regeneration Project, Japan Science and Technology Agency (JST), Tokyo 153-8902, Japan. [3]Institute of Stem Cell Biology and Regenerative Medicine, Stanford University School of Medicine, Stanford, California 94305, USA. [4]Department of Reproductive Biology, National Institute for Child Health and Development, Tokyo 157-8535, Japan. [5]Department of Biochemistry, Graduate School of Biomedical Sciences, Hiroshima University, Hiroshima 734-8551, Japan. [6]Department of Life Sciences (Biology), Graduate School of Arts and Science, The University of Tokyo, Tokyo 153-8902, Japan. [7]National Institute of Advanced Industrial Sciences and Technology (AIST), Ibaraki 305-8562, Japan.
*These authors contributed equally to this work.

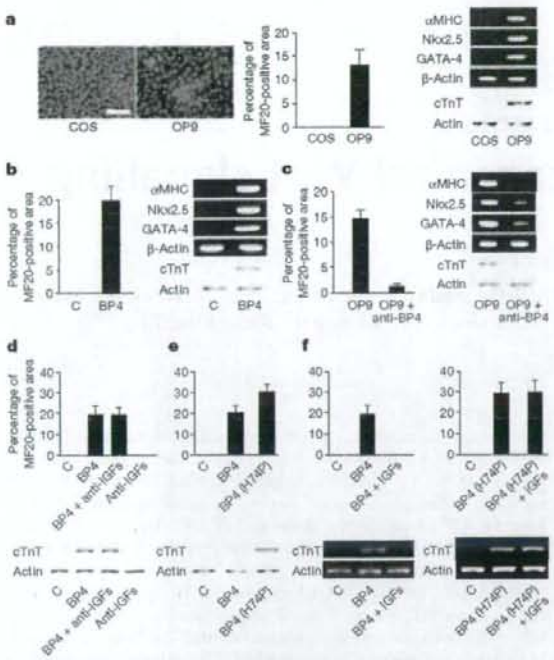

Figure 1 | IGFBP-4 promotes cardiomyocyte differentiation in an IGF-independent manner. a, Culture media conditioned by OP9 cells but not by COS7 cells induced cardiomyocyte differentiation of P19CL6 cells as assessed by MF20-positive area, cardiac marker-gene expression and cTnT protein expression. Scale bar, 100 μm. Error bars show s.d. **b**, Treatment with IGFBP-4 (1 μg ml^{-1}) induced cardiomyocyte differentiation of P19CL6 cells in the absence of DMSO. Error bars show s.d. **c**, Treatment with a neutralizing antibody against IGFBP-4 (anti-BP4; 40 μg ml^{-1}) attenuated cardiomyocyte differentiation of P19CL6 cells induced by OP9-conditioned media. Error bars show s.d. **d**, Treatment with neutralizing antibodies against IGF-I and IGF-II (anti-IGFs; 5 μg ml^{-1} each) had no effect on IGFBP-4-induced cardiomyocyte differentiation of P19CL6 cells. Error bars show s.d. **e**, Mutant IGFBP-4 (BP4(H74P)) that is incapable of binding to IGFs retained cardiomyogenic activity. Error bars show s.d. **f**, IGFs (100 ng ml^{-1} each) attenuated wild-type IGFBP-4-induced but not mutant IGFBP-4-H74P-induced cardiomyocyte differentiation of P19CL6 cells. Error bars show s.d.

that IGFBP-4 induces cardiomyocyte differentiation in an IGF-independent fashion.

To explore further the mechanisms by which IGFBP-4 induces cardiomyogenesis, we tested the hypothesis that IGFBP-4 might modulate the signals activated by other secreted factors implicated in cardiogenesis. It has been shown that canonical Wnt signalling is crucial in cardiomyocyte differentiation[3,4]. In P19CL6 cells, Wnt3A treatment activated β-catenin-dependent transcription of the TOPFLASH reporter gene, and this activation was attenuated by IGFBP-4 (Fig. 2a). Wnt/β-catenin signalling is transduced by the cell-surface receptor complex consisting of Frizzled and low-density-lipoprotein receptor (LDLR)-related protein 5/6 (LRP5/6)[9] and IGFBP-4 attenuated TOPFLASH activity enhanced by the expression of LRP6 or Frizzled 8 (Frz8) (Fig. 2a). As a control, IGFBP-4 did not alter BMP-mediated activation of a BMP-responsive reporter BRE–luc (Supplementary Fig. 1b). These findings suggest that IGFBP-4 is a specific inhibitor of the canonical Wnt pathway. To examine this possibility *in vivo*, we performed axis duplication assays in *Xenopus* embryos. Injection of *Xwnt8* or *Lrp6* mRNA caused secondary axis formation, and injection of *Xenopus IGFBP-4* (*XIGFBP-4*) mRNA alone had minimal effects on axis formation. However, Xwnt8-induced or LRP6-induced secondary axis formation was efficiently blocked by coexpression of XIGFBP-4 (Fig. 2b, c), indicating that IGFBP-4 inhibits canonical Wnt signalling *in vivo*. To explore the mechanisms of Wnt inhibition by IGFBP-4, *Xenopus* animal cap assays and TOPFLASH reporter gene assays were performed. In animal cap assays, IGFBP-4 inhibited LRP6-induced but not β-catenin-induced Wnt-target gene expression (Supplementary Fig. 1c). Similarly, IGFBP-4 attenuated Wnt3A-induced or LRP6-induced TOPFLASH activity but did not alter Dishevelled-1 (Dvl-1)-induced, LiCl-induced or β-catenin-induced TOPFLASH activity (Supplementary Fig. 1d, e). These findings suggest that IGFBP-4 inhibits canonical Wnt signalling at the level of cell-surface receptors. To examine whether IGFBP-4 antagonizes Wnt signalling via direct physical interaction with LRP5/6 or Frizzled, we produced conditioned media containing the Myc-tagged extracellular portion of LRP6 (LRP6N–Myc), the Myc-tagged cysteine-rich domain (CRD) of Frz8 (Frz8CRD–Myc), and V5-tagged IGFBP-4 (IGFBP-4–V5). Immunoprecipitation (IP)/western blot experiments revealed that IGFBP-4 interacted with LRP6N (Fig. 2d) and Frz8CRD (Fig. 2e). A liquid-phase binding assay with ^{125}I-labelled IGFBP-4 and conditioned media containing LRP6N–Myc or Frz8CRD–Myc demonstrated that the interaction between IGFBP-4 and LRP6N or Frz8CRD was specific and saturable (Fig. 2f, g). A Scatchard plot analysis revealed two binding sites with different binding affinities for LRP6N (Fig. 2f, inset) and a single binding site for Frz8CRD (Fig. 2g, inset). A similar binding assay with ^{125}I-labelled Wnt3A demonstrated that IGFBP-4 inhibited Wnt3A binding to LRP6N (Fig. 2h) and Frz8CRD (Fig. 2i), and a Lineweaver–Burk plot revealed that IGFBP-4 was a competitive inhibitor of the binding of Wnt3A to Frz8CDR (Supplementary Fig. 2a). IP/western blot analyses with various deletion mutants of LRP6 and IGFBP-4 revealed that IGFBP-4 interacted with multiple domains of LRP6 and that the carboxy-terminal thyroglobulin domain of IGFBP-4 was required for IGFBP-4 binding to LRP6 or Frz8CRD (Supplementary Fig. 2b–f). It has been shown that inhibition of canonical Wnt signalling promotes cardiomyocyte differentiation in embryonic stem (ES) cells and in chick, *Xenopus* and zebrafish embryos[4,10,11]. These results therefore collectively suggest that IGFBP-4 promotes cardiogenesis by antagonizing the Wnt/β-catenin pathway through direct interactions with Frizzled and LRP5/6.

Next we investigated the role of endogenous IGFBP-4 in P19CL6 cell differentiation into cardiomyocytes. Reverse transcriptase-mediated polymerase chain reaction (RT–PCR) analysis revealed that the expression of *Igfbp4* was upregulated during DMSO-induced P19CL6 cell differentiation (Fig. 3a). Expression of *Igfbp3* and *Igfbp5* was also upregulated in the early and the late phases of differentiation, respectively. Expression of *Igfbp2* was not altered, and that of *Igfbp1* or *Igfbp6* was not detected. When IGFBP-4 was knocked down by two different small interfering RNA (siRNA) constructs, DMSO-induced cardiomyocyte differentiation was inhibited in both cases (Fig. 3b). In contrast, knockdown of *Igfbp3* or *Igfbp5* did not inhibit DMSO-induced cardiomyocyte differentiation (Fig. 3b, right panel). Treatment with an anti-IGFBP-4 neutralizing antibody also blocked DMSO-induced cardiomyocyte differentiation (Fig. 3c). Secretion of endogenous IGFBP-4 is therefore required for the differentiation of P19CL6 cells into cardiomyocytes. Immunostaining for IGFBP-4 revealed that cardiac myocytes were surrounded by the IGFBP-4-positive cells, suggesting that a paracrine effect of IGFBP-4 on cardiomyocyte differentiation is predominant (Fig. 3d). Essentially the same results were obtained in ES cells (Supplementary Fig. 3d–g). To investigate whether IGFBP-4 promotes the differentiation of P19CL6 cells into cardiomyocytes by the inhibition of the canonical Wnt pathway, we expressed dominant-negative LRP6 (LRP6N) in P19CL6 cells. Expression of LRP6N enhanced cardiomyocyte differentiation of P19CL6 cells and reversed the inhibitory effect of *Igfbp4*

knockdown on cardiomyogenesis (Fig. 3e). These observations suggest that endogenous IGFBP-4 is required for cardiomyocyte differentiation of P19CL6 cells and ES cells, and that the cardiogenic effect of IGFBP-4 is mediated by its inhibitory effect on Wnt/β-catenin signalling.

The role of endogenous IGFBP-4 in cardiac development *in vivo* was also examined with *Xenopus* embryos. Whole-mount *in situ* hybridization analysis revealed that strong expression of *XIGFBP-4* was detected at stage 38 in the anterior part of the liver adjacent to the heart (Fig. 4a). Knockdown of *XIGFBP-4* by two different morpholino (MO) constructs resulted in cardiac defects, with more than 70% of the embryos having a small heart or no heart (Fig. 4b). The specificity of MO was confirmed by the observation that simultaneous injection of MO-resistant *XIGFBP-4* cDNA rescued the MO-induced cardiac defects (Fig. 4b, Supplementary Fig. 4c). Coexpression of IGF-binding-defective XIGFBP-4 mutant (XIGFBP-4-H74P) or dominant-negative LRP6 (LRP6N) also rescued the cardiac defects induced by *XIGFBP-4* knockdown (Fig. 4b), whereas overexpression of Xwnt8 in the heart-forming region resulted in cardiac defects similar to those induced by *XIGFBP-4* knockdown (Supplementary Fig. 4d–f), supporting the notion that the cardiogenic effect of IGFBP-4 is independent of IGFs but is mediated by inhibition of the Wnt/β-catenin pathway. The temporal profile of cardiac defects induced by *XIGFBP-4* knockdown was also examined by *in situ* hybridization with *cardiac troponin I* (*cTnI*) (Fig. 4c). At stage 34, morphology of the heart was comparable between control embryos and MO-injected embryos. However, at stage 38, when *XIGFBP-4* starts to be expressed in the anterior part of the liver, the expression of *cTnI* was markedly attenuated in MO-injected embryos; expression of *cTnI* was diminished and no heart-like structure was observed at stage 42. Thus, the heart is initially formed but its subsequent growth is perturbed in the absence of XIGFBP-4, suggesting that IGFBP-4

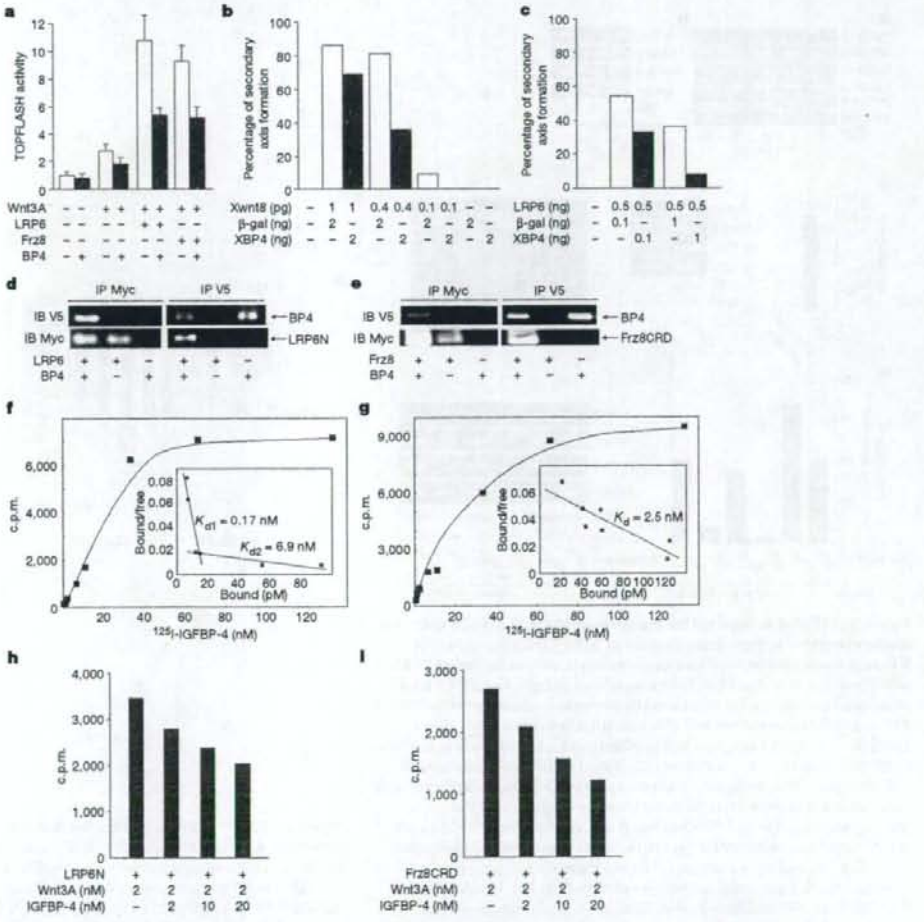

Figure 2 | IGFBP-4 inhibits Wnt/β-catenin signalling through direct interactions with Wnt receptors. **a**, IGFBP-4 attenuated β-catenin-dependent transcription in P19CL6 cells. P19CL6 cells were transfected with TOPFLASH reporter gene and expression vectors for LRP6 or Frz8, and then treated with Wnt3A or Wnt3A plus IGFBP-4; luciferase activities were then measured. Error bars show s.d. **b**, XIGFBP-4 (XBP4) inhibited Xwnt8-induced secondary-axis formation in *Xenopus* embryos ($n = 20$ for each group). **c**, IGFBP-4 inhibited LRP6-induced secondary-axis formation in *Xenopus* embryos ($n = 30$ for each group). **d**, **e**, IGFBP-4 interacted directly with LRP6N (**d**) and Frz8CRD (**e**). IB, immunoblotting; IP, immunoprecipitation. **f**, A binding assay between ^{125}I-labelled IGFBP-4 and LRP6N. The inset is a Scatchard plot showing two binding sites with different binding affinities. **g**, A binding assay between ^{125}I-labelled IGFBP-4 and Frz8CRD. The inset is a Scatchard plot showing a single binding site. **h**, **i**, IGFBP-4 inhibited Wnt3A binding to LRP6N (**h**) or Frz8CRD (**i**). ^{125}I-labelled Wnt3A binding to LRP6N or Frz8CRD was assessed in the presence of increasing amounts of IGFBP-4.

promotes cardiogenesis by maintaining the proliferation and/or survival of embryonic cardiomyocytes.

It has been shown that canonical Wnt signals inhibit cardiogenesis in chick and frog embryos, and that Wnt antagonists such as Dkk1 and Crescent secreted from the anterior endoderm or the organizer region counteract the Wnt-mediated inhibitory signals and induce cardiogenesis in the anterior lateral mesoderm[4]. However, IGFBP-4-mediated Wnt inhibition is required at later stages of development, when the heart is already formed at the ventral portion and starts to grow and remodel to maintain embryonic circulation. It has been shown that Wnt/β-catenin signalling has time-dependent effects on cardiogenesis in ES cells: canonical Wnt signalling in the early phase of ES-cell differentiation promotes cardiomyogenesis, whereas it inhibits cardiomyocyte differentiation in the late phase[10–12]. In agreement with this notion, IGFBP-4 promoted cardiomyocyte differentiation of ES cells only when IGFBP-4 was applied in the late phase after embryoid body formation (Supplementary Fig. 3a–c). Similar time-dependent effects of Wnt/β-catenin signalling on cardiogenesis has been shown in zebrafish embryos[11]. Moreover, several recent reports suggest that Wnt/β-catenin signalling is a positive regulator of cardiac progenitor-cell proliferation in the secondary heart field[13]. It therefore seems that canonical Wnt signalling has divergent effects on cardiogenesis at multiple stages of development: first, canonical Wnt signalling promotes cardiogenesis at the time of gastrulation or mesoderm specification; second, it inhibits cardiogenesis at the time when cardiac mesoderm is specified in the anterior lateral mesoderm; third, it promotes the expansion of cardiac progenitors in the secondary heart field; and fourth, it inhibits cardiogenesis at later stages when the embryonic heart is growing. It is interesting to note that IGFBP-4 is expressed predominantly in the liver. Mouse IGFBP-4 is

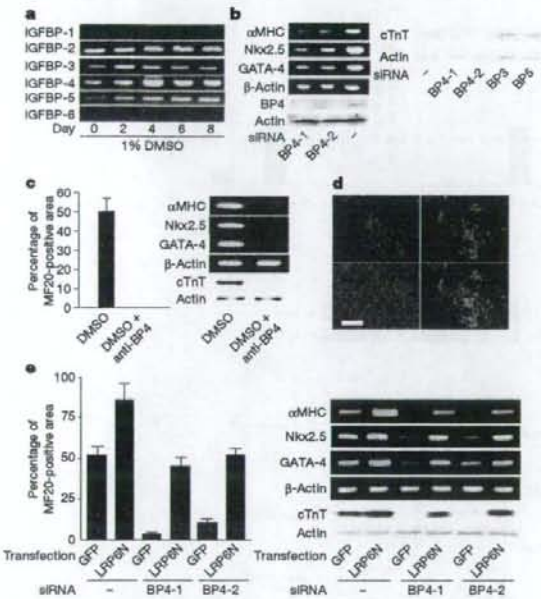

Figure 3 | IGFBP-4 is required for the differentiation of P19CL6 cells into cardiomyocytes. **a**, Expression analysis of IGFBP family members by RT–PCR during DMSO-induced cardiomyocyte differentiation of P19CL6 cells (from day 0 to day 8). **b**, Left: knockdown of *Igfbp4* in P19CL6 cells attenuated cardiac marker expression in response to treatment with DMSO. BP4-1 and BP4-2 represent two different siRNAs for IGFBP-4. Right: knockdown of *Igfbp3* or *Igfbp5* had no effect on cTnT expression in response to DMSO treatment. **c**, Treatment with a neutralizing antibody against IGFBP-4 (anti-BP4; 40 μg ml^{-1}) attenuated DMSO-induced cardiomyocyte differentiation of P19CL6 cells. Error bars show s.d. **d**, IGFBP-4 immunostaining during DMSO-induced differentiation of P19CL6 cells stably transfected with αMHC–green fluorescent protein (GFP) reporter gene. Top left, IGFBP-4 staining (red); top right, GFP expression representing differentiated cardiomyocytes; bottom left, nuclear staining with DAPI (4′,6-diamidino-2-phenylindole); bottom right, a merged picture. Scale bar, 100 μm. **e**, Attenuated cardiomyocyte differentiation of P19CL6 cells by *Igfbp4* knockdown was rescued by inhibiting Wnt/β-catenin signalling. Control and *Igfbp4*-knocked-down P19CL6 cells were transfected with an expression vector for GFP or LRP6N (a dominant-negative form of LRP6) and induced to differentiate into cardiomyocytes by treatment with DMSO. LRP6N overexpression rescued the attenuated cardiomyocyte differentiation induced by *Igfbp4* knockdown as assessed by MF20-positive area (left panel), cardiac marker-gene expression and cTnT protein expression (right panel). Error bars show s.d.

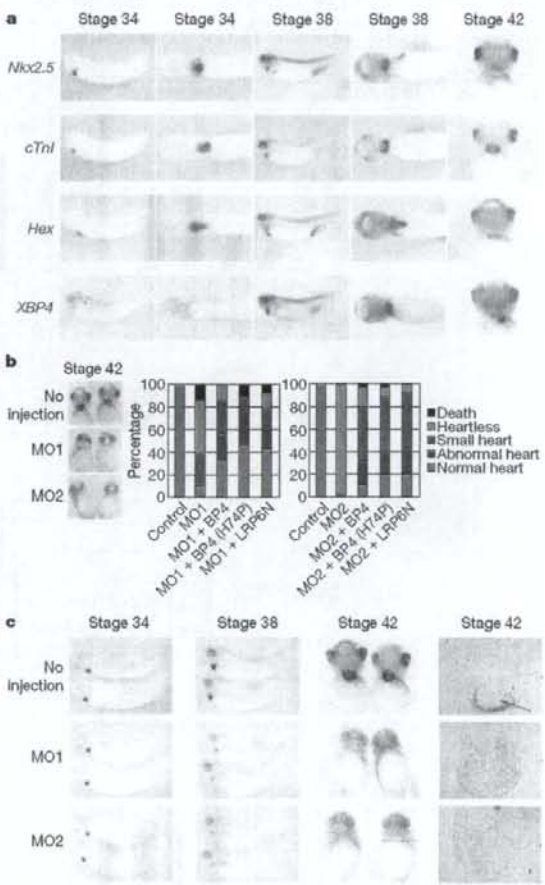

Figure 4 | IGFBP-4 is required for the maturation of the heart in *Xenopus* embryos. **a**, *In situ* hybridization analysis of *Nkx2.5* (an early cardiac marker), *cTnI* (a mature cardiac marker), *Hex* (a liver marker), and *XIGFBP-4* (*XBP4*) mRNA expression at stages 34, 38 and 42. **b**, Knockdown of *XIGFBP-4* by two different morpholinos (MO1 and MO2) resulted in severe cardiac defects as assessed by *cTnI in situ* hybridization at stage 42 (left). These cardiac defects were rescued by simultaneous injection of MO-resistant wild-type XIGFBP-4, mutant XIGFBP-4-H74P (BP4(H74P) and LRP6N ($n = 30$ for each group). **c**, Temporal profile of cardiac defects induced by *XIGFBP-4* knockdown. Morphology of the heart as assessed by cTnI *in situ* hybridization was almost normal at stage 34 but was severely perturbed at stages 38 and 42. The right column shows sections of control and MO-injected embryos. The arrow indicates the heart in control embryos. No heart-like structure was observed in MO-injected embryos.

also strongly expressed in the tissues adjacent to the heart such as pharyngeal arches and liver bud at embryonic day (E)9.5 (Supplementary Fig. 3h). These observations and the results of IGFBP-4 immunostaining in P19CL6 cells and ES cells suggest that IGFBP-4 promotes cardiogenesis in a paracrine fashion. Together with a previous report showing that cardiac mesoderm secretes FGFs and induces liver progenitors in the ventral endoderm[14], these observations suggest that there exist reciprocal paracrine signals between the heart and the liver that coordinately promote the development of each other.

IGFBPs are composed of six members, IGFBP-1 to IGFBP-6. Reporter gene assays and β-catenin stabilization assays revealed that IGFBP-4 was the most potent canonical Wnt inhibitor and that IGFBP-1, IGFBP-2 and IGFBP-6 also showed modest activity in Wnt inhibition, whereas IGFBP-3 and IGFBP-5 had no such activity (Supplementary Fig. 5a–c). In agreement with this, IP/western blot analyses demonstrated that IGFBP-1, IGFBP-2, IGFBP-4 and IGFBP-6 but not IGFBP-3 or IGFBP-5 interacted with LRP6 or Frz8CRD (Supplementary Fig. 5d, e). Thus, the lack of cardiac phenotypes in IGFBP-4-null mice or IGFBP-3/IGFBP-4/IGFBP-5 triple knockout mice[15] may be due to genetic redundancies between IGFBP-4 and other IGFBPs such as IGFBP-1, IGFBP-2 and/or IGFBP-6.

The identification of IGFBP-4 as an inhibitor of Wnt/β-catenin signalling may also have some implications for cancer biology[16]. It was shown that treatment with IGFBP-4 reduces cell proliferation in some cancer cell lines *in vitro*, and that overexpression of IGFBP-4 attenuates the growth of prostate cancer *in vivo*. Decreased serum levels of IGFBP-4 are associated with the risk of breast cancer. Because the activation of Wnt signalling is implicated in several forms of malignant tumours[17,18], it is possible that the inhibitory effect of IGFBP-4 on cell proliferation is mediated in part by the inhibition of canonical Wnt signalling.

METHODS SUMMARY

Cell culture. P19CL6 cells and ES cells were cultured and induced to differentiate into cardiomyocytes essentially as described[8,19]. P19CL6 cells (2,000 cells per 35-mm dish) were treated with various conditioned media for screening of their cardiogenic activities. For siRNA-mediated knockdown, pSIREN-RetroQ vectors (Clontech) ligated with double-stranded oligonucleotides were transfected into P19CL6 cells or ES cells, and puromycin-resistant clones were selected.

IP/western blot analyses and binding assays. Conditioned media for IP/western blot analyses were produced by using 293 cells. Binding reactions were performed overnight at 4 °C. ^{125}I-labelling of IGFBP-4 and Wnt3A was performed with IODO-BEADS Iodination Reagent (Pierce). A liquid-phase binding assay was performed essentially as described[19].

***Xenopus* experiments.** Axis duplication assays, animal cap assays, and *in situ* hybridization analyses in *Xenopus* were performed essentially as described[20]. Electroporation of mRNA was performed at stage 28 essentially as described[21].

Full Methods and any associated references are available in the online version of the paper at www.nature.com/nature.

Received 22 August 2007; accepted 24 April 2008.
Published online 4 Jun 2008.

1. Firth, S. M. & Baxter, R. C. Cellular actions of the insulin-like growth factor binding proteins. *Endocr. Rev.* 23, 824–854 (2002).
2. Mohan, S. & Baylink, D. J. IGF-binding proteins are multifunctional and act via IGF-dependent and -independent mechanisms. *J. Endocrinol.* 175, 19–31 (2002).
3. Olson, E. N. & Schneider, M. D. Sizing up the heart: development redux in disease. *Genes Dev.* 17, 1937–1956 (2003).
4. Foley, A. & Mercola, M. Heart induction: embryology to cardiomyocyte regeneration. *Trends Cardiovasc. Med.* 14, 121–125 (2004).
5. Leri, A., Kajstura, J. & Anversa, P. Cardiac stem cells and mechanisms of myocardial regeneration. *Physiol. Rev.* 85, 1373–1416 (2005).
6. Monzen, K. *et al.* Bone morphogenetic proteins induce cardiomyocyte differentiation through the mitogen-activated protein kinase kinase kinase TAK1 and cardiac transcription factors Csx/Nkx-2.5 and GATA-4. *Mol. Cell. Biol.* 19, 7096–7105 (1999).
7. Ueno, H. *et al.* A stromal cell-derived membrane protein that supports hematopoietic stem cells. *Nature Immunol.* 4, 457–463 (2003).
8. Qin, X., Strong, D. D., Baylink, D. J. & Mohan, S. Structure-function analysis of the human insulin-like growth factor binding protein-4. *J. Biol. Chem.* 273, 23509–23516 (1998).
9. Moon, R. T., Kohn, A. D., De Ferrari, G. V. & Kaykas, A. WNT and β-catenin signalling: diseases and therapies. *Nature Rev. Genet.* 5, 691–701 (2004).
10. Naito, A. T. *et al.* Developmental stage-specific biphasic roles of Wnt/β-catenin signaling in cardiomyogenesis and hematopoiesis. *Proc. Natl Acad. Sci. USA* 103, 19812–19817 (2006).
11. Ueno, S. *et al.* Biphasic role for Wnt/β-catenin signaling in cardiac specification in zebrafish and embryonic stem cells. *Proc. Natl Acad. Sci. USA* 104, 9685–9690 (2007).
12. Liu, Y. *et al.* Sox17 is essential for the specification of cardiac mesoderm in embryonic stem cells. *Proc. Natl Acad. Sci. USA* 104, 3859–3864 (2007).
13. Cohen, E. D., Tian, Y. & Morrisey, E. E. Wnt signaling: an essential regulator of cardiovascular differentiation, morphogenesis and progenitor self-renewal. *Development* 135, 789–798 (2008).
14. Jung, J., Zheng, M., Goldfarb, M. & Zaret, K. S. Initiation of mammalian liver development from endoderm by fibroblast growth factors. *Science* 284, 1998–2003 (1999).
15. Ning, Y. *et al.* Diminished growth and enhanced glucose metabolism in triple knockout mice containing mutations of insulin-like growth factor binding protein-3, -4, and -5. *Mol. Endocrinol.* 20, 2173–2186 (2006).
16. Durai, R. *et al.* Biology of insulin-like growth factor binding protein-4 and its role in cancer. *Int. J. Oncol.* 28, 1317–1325 (2006).
17. Logan, C. Y. & Nusse, R. The Wnt signaling pathway in development and disease. *Annu. Rev. Cell Dev. Biol.* 20, 781–810 (2004).
18. Clevers, H. Wnt/β-catenin signaling in development and disease. *Cell* 127, 469–480 (2006).
19. Semenov, M. V. *et al.* Head inducer Dickkopf-1 is a ligand for Wnt coreceptor LRP6. *Curr. Biol.* 11, 951–961 (2001).
20. Kobayashi, H. *et al.* Novel Daple-like protein positively regulates both the Wnt/β-catenin pathway and the Wnt/JNK pathway in *Xenopus*. *Mech. Dev.* 122, 1138–1153 (2005).
21. Sasagawa, S., Takabatake, T., Takabatake, Y., Muramatsu, T. & Takeshima, K. Improved mRNA electroporation method for *Xenopus* neurula embryos. *Genesis* 33, 81–85 (2002).

Supplementary Information is linked to the online version of the paper at www.nature.com/nature.

Acknowledgements We thank E. Fujita, R. Kobayashi and Y. Ishiyama for technical support; T. Yamauchi and K. Ueki for advice on binding assays; and Y. Onuma and S. Takahashi for advice on *Xenopus* electroporation. This work was supported by grants from the Ministry of Education, Culture, Sports, Science and Technology (MEXT), the Ministry of Health, Labour, and Welfare, and the New Energy and Industrial Technology Development Organization (NEDO).

Author Contributions W.Z., I.S. and Y.I. contributed equally to this work. I.K. designed and supervised the research. W.Z., I.S., Y.I., Z.L., H.I., M.Y. and A.T.N. performed experiments. J.N., H.U., A.U., T.M., T.N., A.K. and M.A. contributed new reagents and/or analytical tools. W.Z., I.S., Y.I., A.K. and I.K. analysed data. W.Z., I.S., Y.I. and I.K. prepared the manuscript.

Author Information Reprints and permissions information is available at www.nature.com/reprints. Correspondence and requests for materials should be addressed to I.K. (komuro-tky@umin.ac.jp).

METHODS

Plasmids and reagents. cDNA clones encoding mouse IGFBPs and *Xenopus* IGFBP-4 were purchased from Open Biosystems. XIGFBP-4-H74P mutant was generated with a QuickChange Site-Directed Mutagenesis kit (Stratagene). His-tagged human wild-type IGFBP-4 and mutant IGFBP-4-H74P (vectors provided by X. Qin)[9] were produced and purified with HisTrap HP Kit (Amersham). Full-length Frz8, Frz8CRD and LRP6N were provided by X. He[22,23]. Full-length LRP6, membrane-bound forms of LRP6 deletion mutants, and Dkk1 were from C. Niehrs[24]. pXwnt8 and pCSKA-Xwnt8 were from J. Christian[25]. pCS2-β-catenin was from D. Kimelman[26]. αMHC–GFP was from B. Fleischmann[27]. BRE–luc was from P. ten Dijke[28]. pCGN-Dvl-1 was described previously[29]. Soluble forms of LRP6 deletion mutants and probes for *in situ* hybridization analysis (Nkx2.5, cTnI and Hex) were generated by PCR. IGFBP-4, Wnt3A, IGF-I, IGF-II and BMP2 were from R&D. Neutralizing antibodies were from R&D (anti-IGFBP-4), Sigma (anti-IGF-I and anti-IGF-II), and Oncogene (anti-type-I IGF receptor). The antibodies used for immunoprecipitation, western blotting and immunostaining were from Invitrogen (anti-Myc, anti-V5), Santa Cruz (anti-cTnT, anti-IGFBP-4, anti-topoisomerase I (TOPO-I)), Sigma (anti-β-actin, anti-β-catenin, anti-FLAG (M2)) and Developmental Studies Hybridoma Bank (anti-sarcomeric myosin heavy chain (MF20)).

Cell culture experiments. P19CL6 cells and ES cells were cultured and induced to differentiate into cardiomyocytes essentially as described[6,10]. P19CL6 cells (2,000 cells per 35-mm dish) were treated with various conditioned media for screening of their cardiogenic activities. P19CL6 cells or ES cells stably transfected with αMHC promoter driven–GFP were generated by transfection of αMHC–GFP plasmid into P19CL6 cells or ht7 ES cells followed by G418 selection. Luciferase reporter gene assays, western blot analyses, immunostaining and RT–PCR were performed as described[30]. Reporter gene assays were repeated at least three times. PCR primers and PCR conditions are listed in Supplementary Table 1. For siRNA-mediated knockdown, siRNAs were expressed with pSIREN-RetroQ vector (Clontech). Oligonucleotide sequences used are listed in Supplementary Table 2. pSIREN-RetroQ vectors ligated with double-stranded oligonucleotides were transfected into P19CL6 cells or ES cells, and puromycin-resistant clones were isolated and expanded. For β-catenin stabilization assays, nuclear extracts of L cells were prepared with NE-PER Nuclear and Cytoplasmic Extraction Reagents (Pierce). Data are shown as means and s.d.

IP/western blot analyses and binding assays. Conditioned media for IP/western blot analyses containing full-length or various deletion mutants of IGFBPs, LRP6, Frz8CRD and Dkk1 were produced with 293 cells. Binding reactions were performed overnight at 4 °C. Immunoprecipitation was performed with Protein G–Sepharose 4 Fast Flow (Amersham). ^{125}I-labelling of IGFBP-4 and Wnt3A was performed with IODO-BEADS Iodination Reagent (Pierce). A liquid-phase binding assay was performed essentially as described[18]. In brief, conditioned media containing LRP6N–Myc or Frz8CRD–Myc were mixed with various concentrations of ^{125}I-labelled IGFBP-4 and incubated overnight at 4 °C. LRP6N–Myc or Frz8CRD–Myc was immunoprecipitated and the radioactivity of bound IGFBP-4 was measured after extensive washing of the Protein G–Sepharose beads. For a competitive binding assay, conditioned media containing LRP6N–Myc or Frz8CRD–Myc were mixed with ^{125}I-labelled Wnt3A and unlabelled IGFBP-4, and incubated overnight at 4 °C. LRP6N–Myc or Frz8CRD–Myc was then immunoprecipitated and the radioactivity of bound Wnt3A was measured.

***Xenopus* experiments and mouse *in situ* hybridization analysis.** Axis duplication assays, animal cap assays and *in situ* hybridization analyses in *Xenopus* were performed essentially as described[30]. Two independent cDNAs for *XIGFBP-4*, presumably resulting from pseudotetraploid genomes, were identified by 5′ rapid amplification of cDNA ends (Supplementary Fig. 4a). Two different MOs targeting both of these two IGFBP-4 transcripts were designed (Gene Tools) (Supplementary Fig. 4a and Supplementary Table 2). MO-sensitive *XIGFBP-4* cDNA including a 41-base-pair 5′-untranslated region (UTR) was generated by PCR. MO-resistant *XIGFBP-4* cDNA (wild-type and H74P mutant) was generated by introducing five silent mutations in the MO1 target sequence and excluding the 5′-UTR (Supplementary Fig. 4a). To determine the specificity of MOs, MO-sensitive or MO-resistant *XIGFBP-4–myc* mRNA was injected into *Xenopus* embryos with or without MOs, and protein/mRNA expression was analysed. PCR primers and PCR conditions are listed in Supplementary Table 1. MOs and plasmid DNAs were injected at the eight-cell stage into the dorsal region of two dorsal–vegetal blastomeres fated to be heart and liver anlage. Electroporation of mRNA was performed essentially as described[31]. Injection of mRNA (5 ng in 5 nl of solution) into the vicinity of heart anlage and application of electric pulses were performed at stage 28. Whole-mount *in situ* hybridization analysis of murine IGFBP-4 was performed as described[30].

22. He, X. *et al.* A member of the Frizzled protein family mediating axis induction by Wnt-5A. *Science* **275**, 1652–1654 (1997).
23. Tamai, K. *et al.* LDL-receptor-related proteins in Wnt signal transduction. *Nature* **407**, 530–535 (2000).
24. Mao, B. *et al.* LDL-receptor-related protein 6 is a receptor for Dickkopf proteins. *Nature* **411**, 321–325 (2001).
25. Christian, J. L. & Moon, R. T. Interactions between Xwnt-8 and Spemann organizer signaling pathways generate dorsoventral pattern in the embryonic mesoderm of *Xenopus*. *Genes Dev.* **7**, 13–28 (1993).
26. Yost, C. *et al.* The axis-inducing activity, stability, and subcellular distribution of β-catenin is regulated in *Xenopus* embryos by glycogen synthase kinase 3. *Genes Dev.* **10**, 1443–1454 (1996).
27. Kolossov, E. *et al.* Identification and characterization of embryonic stem cell-derived pacemaker and atrial cardiomyocytes. *FASEB J.* **19**, 577–579 (2005).
28. Korchynskyi, O. & ten Dijke, P. Identification and functional characterization of distinct critically important bone morphogenetic protein-specific response elements in the Id1 promoter. *J. Biol. Chem.* **277**, 4883–4891 (2002).
29. Kishida, M. *et al.* Synergistic activation of the Wnt signaling pathway by Dvl and casein kinase Iε. *J. Biol. Chem.* **276**, 33147–33155 (2001).
30. Hosoda, T. *et al.* A novel myocyte-specific gene Midori promotes the differentiation of P19CL6 cells into cardiomyocytes. *J. Biol. Chem.* **276**, 35978–35989 (2001).

STEM CELLS

TISSUE-SPECIFIC STEM CELLS

Novel Cardiac Precursor-Like Cells from Human Menstrual Blood-Derived Mesenchymal Cells

NAOKO HIDA,[a,b,c] NOBUHIRO NISHIYAMA,[a,c] SHUNICHIRO MIYOSHI,[a,d] SHINICHIRO KIRA,[a] KAORU SEGAWA,[e] TARO UYAMA,[b] TAISUKE MORI,[c] KENJI MIYADO,[b] YUKINORI IKEGAMI,[a,b] CHANGHAO CUI,[b] TOHRU KIYONO,[f] SATORU KYO,[g] TATSUYA SHIMIZU,[h] TERUO OKANO,[h] MICHIE SAKAMOTO,[c] SATOSHI OGAWA,[a] AKIHIRO UMEZAWA[b]

[a]Department of Cardiology, Keio University School of Medicine, Tokyo, Japan; [b]Department of Reproductive Biology and Pathology, National Research Institute for Child Health and Development, Tokyo, Japan; [c]Department of Pathology, Keio University School of Medicine, Tokyo, Japan; [d]Institute for Advanced Cardiac Therapeutics, Keio University School of Medicine, Tokyo, Japan; [e]Department of Microbiology and Immunology, Keio University School of Medicine, Tokyo, Japan; [f]Virology Division, National Cancer Center Research Institute, Tokyo, Japan; [g]Department of Obstetrics and Gynecology, Kanazawa University, School of Medicine, Kanazawa, Japan; [h]Institute of Advanced Biomedical Engineering and Science, Tokyo Women's Medical University, Tokyo, Japan

Key Words. Cardiomyogenesis human mesenchymal stem cell • Menstrual blood endometrial gland • Cell sheet technology cardiac precursors

ABSTRACT

Stem cell therapy can help repair damaged heart tissue. Yet many of the suitable cells currently identified for human use are difficult to obtain and involve invasive procedures. In our search for novel stem cells with a higher cardiomyogenic potential than those available from bone marrow, we discovered that potent cardiac precursor-like cells can be harvested from human menstrual blood. This represents a new, noninvasive, and potent source of cardiac stem cell therapeutic material. We demonstrate that menstrual blood-derived mesenchymal cells (MMCs) began beating spontaneously after induction, exhibiting cardiomyocyte-specific action potentials. Cardiac troponin-I-positive cardiomyocytes accounted for 27%–32% of the MMCs in vitro. The MMCs proliferated, on average, 28 generations without affecting cardiomyogenic transdifferentiation ability, and expressed mRNA of GATA-4 before cardiomyogenic induction. Hypothesizing that the majority of cardiomyogenic cells in MMCs originated from detached uterine endometrial glands, we established monoclonal endometrial gland-derived mesenchymal cells (EMCs), 76%–97% of which transdifferentiated into cardiac cells in vitro. Both EMCs and MMCs were positive for CD29, CD105 and negative for CD34, CD45. EMCs engrafted onto a recipient's heart using a novel 3-dimensional EMC cell sheet manipulation transdifferentiated into cardiac tissue layer in vivo. Transplanted MMCs also significantly restored impaired cardiac function, decreasing the myocardial infarction (MI) area in the nude rat model, with tissue of MMC-derived cardiomyocytes observed in the MI area in vivo. Thus, MMCs appear to be a potential novel, easily accessible source of material for cardiac stem cell-based therapy. STEM CELLS *2008;26:1695–1704*

Disclosure of potential conflicts of interest is found at the end of this article.

INTRODUCTION

Marrow-derived mesenchymal stem cells (MSCs) are a potential cellular source for stem cell-based therapy, since they have the ability to differentiate into cardiomyocytes [1, 2], use of MSCs presents no ethical problems, and autologous MSCs have been injected into ischemic hearts clinically [3]. Direct injection of MSCs into the heart has been shown to be feasible in vivo [4–7], but with limited effect. The reason for this may be the extremely low rate of cardiomyogenesis exhibited by marrow-derived MSCs [2], with cardiac function improvement due to grafted MSC-induced neovascularization [7, 8] and an antiapoptotic

Author contributions: N.H.: conception and design, collection and assembly of data, data analysis and interpretation, final approval of manuscript; N.N.: conception and design, collection and assembly of data, data analysis and interpretation, manuscript writing, final approval of manuscript; S.M.: conception and design, administrative support, collection and assembly of data, data analysis and interpretation, manuscript writing, final approval of manuscript; S. Kira and Y.I.: collection and assembly of data, final approval of manuscript; K.S., C.C., T.K., S. Kyo, and T.S.: provision of study material, final approval of manuscript; T.U.: provision of study material, collection and assembly of data, final approval of manuscript; T.M.: collection and assembly of data, data analysis and interpretation, final approval of manuscript; K.M.: collection and assembly of data, final approval of manuscript; T.O.: administrative support, provision of study material, final approval of manuscript; M.S.: administrative support, final approval of manuscript; S.O.: financial support, administrative support, final approval of manuscript; A.U.: financial support, administrative support, manuscript writing, final approval of manuscript.

Correspondence: Shunichiro Miyoshi M.D., Ph.D., Keio University School of Medicine, 35-Shinanomachi, Shinjuku-ku, Tokyo, 160-8582 Japan. Telephone: +81-3-3353-1211 (ext 62310); Fax: +81-3-3353-2502; e-mail: smiyoshi@cpnet.med.keio.ac.jp Received October 2, 2007; accepted for publication April 6, 2008; first published online in STEM CELLS *EXPRESS* April 17, 2008.
1066-5099/2008/$30.00/0 doi: 10.1634/stemcells.2007-0826

effect on infarcted cardiomyocytes [9, 10]. To further improve prospects of restoring cardiac function, a search was initiated for another source of cells having high cardiomyogenic potential.

Our previous study showed that umbilical cord blood-derived mesenchymal stem cells (UCBMSCs) [11] and placental chorionic plate cells (PCPCs) [12] have a phenotype of mesenchymal cells and have higher cardiomyogenic differentiation ability in vitro. Since these materials are deemed medical waste and can be obtained without any ethical problems, they may be a suitable stem cell source for cardiac regenerative therapy. But the population of UCBMSCs in umbilical cord blood is scant [13] and there is also a problem in establishing PCPCs, since placental tissue contains a lot of maternal decidua-derived mesenchymal cells that could contaminate PCPCs. Therefore, it is difficult to obtain enough of these cells without using a limiting dilution method and/or massive ex vivo propagation, which may cause instability of the genome [14]. Consequently, material that contains a large amount of mesenchymal cells during the first few passages should be a highly suitable source of stem cells.

A previous paper suggests that endometrium contains an MSC-like population [15] and menstrual blood-derived mesenchymal (MMCs) cells have a pluripotent differentiation ability in vitro [16]. The data presented here demonstrate that human menstrual blood-derived mesenchymal cells and uterine endometrial gland-derived mesenchymal cells (EMCs) have a strong potential for cardiomyogenic transdifferentiation in vitro and in vivo. Moreover, large amounts of MMCs could be obtained from the first passage of menstrual blood culture, and MMCs have been shown to restore impaired cardiac function through marked cardiomyogenesis in vivo.

MATERIALS AND METHODS

Isolation of MMCs and EMCs

After informed consent was obtained, mesenchymal cells from approximately 10 ml of menstrual blood of six women (20–30 years old) were collected on the first day of menstruation. The samples were suspended in Dulbecco's modified Eagle's medium (DMEM) high glucose supplemented with 10% FBS, and split into two 10-cm dishes. The estimated adherent cell number at the start of culture was approximately 1×10^7. The growth curve and phase-contrast microscopic view are shown in supplemental online Fig. 1. The results for MMCs obtained from six women were the same. A human endometrial tissue sample was also taken from a 52-year-old woman undergoing hysterectomy [17]. Individual endometrial glands were isolated under a microscope and then seeded. After the retroviral transfection of HPV16E6, E7, and hTERT [2], endometrial cell strains were generated by the limiting dilution method. Two strains exhibiting rapid cell division cycles were designated EMC100 and EMC214 (Fig. 3B and 3D, respectively). EMC100 and EMC214 showed adherent spindle shape morphology that proliferated for more than 250 population doublings without changing cardiomyogenic differentiation ability.

Isolation of Marrow-Derived Mesenchymal Stem Cells

Bone marrow-derived mesenchymal stem cells (BMMSCs) were obtained from a 41-year-old male as described previously [2].

Coculture with Murine Fetal Cardiomyocytes

MMCs, EMCs, and BMMSCs were infected with enhanced green fluorescent protein (EGFP) expressing adenovirus [2]. Fetal cardiomyocytes were obtained from hearts of day-17 mouse fetuses, as previously described [2]. The isolated cardiomyocytes were replated at $5 \times 10^4/cm^2$ on top of a floating athelocollagen membrane (CM-6, 40-μm thickness; Koken, Tokyo, http://www.kokenmpc.co.jp/english/products/collagen/cell_culture/cm-6_24/index.html) that is permeable for only small molecules (less than 5,000 MW). The next day, the athelocollagen membrane was plated upside down on the culture dish. Harvested EGFP-labeled MMCs and EMCs were then seeded upon the athelocollagen surface (bottom surface) at $7 \times 10^3/cm^2$ (Fig. 1M). In several experiments (Figs. 1G–1L, 2, 3E, 3H, 3K–3M, 4, supplemental online Fig. 2, examination of chromosome chimeras), we did not use the athelocollagen membrane for the coculture system.

Immunocytochemistry and Immunohistochemistry

A laser confocal microscope (FV1000; Olympus, Tokyo, http://www.olympus-global.com) was used for immunocytochemical analysis. Samples were stained with mouse monoclonal anti-cardiac troponin-I antibody (4T21 Lot 98/10-T21-C2; HyTest, Euro, Finland, http://www.hytest.fi/) or with mouse monoclonal anti-sarcomeric α-actinin antibody (Sigma-Aldrich, St. Louis, http://www.sigmaaldrich.com), or anti-connexin 43 antibody (Sigma-Aldrich) diluted 1:300 overnight at 4°C, then stained with TRITC-conjugated anti-mouse antibody (Sigma-Aldrich), TRITC-conjugated anti-rabbit antibody (Sigma-Aldrich), and Cy5-conjugated anti-mouse IgG (Chemicon, Temecula, CA, http://www.chemicon.com) diluted 1:100, containing 4′-6-diamidino-2-phenylindole (DAPI; Wako Chemical, Osaka, Japan, http://www.wako-chem.co.jp/english) at 1:300 for 30 minutes at 25°C–28°C. See also supplemental online data 1 for detail of method.

Functional Analysis

The method of action potential (AP) recording was as previously described [2] but with slight modification. A fluorescence inverted microscope (IX-70; Olympus) was used for AP recording. The microscope was equipped with a recording chamber and a noiseless heating plate (Microwarm Plate; Kitazato Supply, Fujinomiya, Shizuoka, Japan, http://www.kitazato-supply.com). A 10-mM volume of HEPES (Sigma-Aldrich) was added to the culture medium to stabilize the pH of the perfusate at 7.5. Standard glass microelectrodes having a direct current resistance of 15–25 MΩ when filled with pipette solution were used. Alexa 568 compound was dissolved to a concentration of 0.5 mM in 2 M of KCl solution in order to completely dissolve the Alexa 568 in the pipette solution. The electrodes were positioned with a motor-driven micromanipulator (PCS-5000; Burleigh Instrument, Inc., New York) under optical control. Spontaneously beating EGFP-positive cells were selected as targets, and after the APs of the target cells had been recorded, the dye was injected by iontophoresis (−7 nA for 10–20 seconds). The extent of dye transfer was monitored under a fluorescence microscope, and digital images were recorded with a digital photo camera (EOS-digital; Canon, Tokyo, http://www.canon.com) mounted on the microscope. The recording pipette was connected to a patch-clamp amplifier (MEZ-8300; Nihon Kohden, Tokyo, http://www.nihonkohden.com). The amplified signal was filtered with a 4-pole Bessel filter (NF-3625; NF electronic instrument; NF Corp., Tokyo, http://www.nfcorp.co.jp/english/index.html) set at 2 kHz, then digitized with an A/D converter with a sampling frequency of 10 kHz (Digidata 1.322A; Molecular Devices Corp., Union City, CA, http://www.moleculardevices.com). Pacemaker potential was defined by the slowly depolarizing membrane potential at phase IV of the AP.

Alexa 568 was injected into cells via recording microelectrodes to stain the cells and confirm that the AP was generated by EGFP-positive cells (Fig. 1G–1I, 3E, 3H). Since the dye did not diffuse into the EGFP-negative murine cardiomyocytes, there were no tight cell-to-cell heterologous connections (i.e., gap junctions), at least in the in vitro condition. In some experiments, Alexa 568 diffused into the EGFP-positive satellite EMCs and MMCs, suggesting that a homologous cell-to-cell connection had been established at least 1 week after cocultivation. The measured parameters of the APs were averaged and are shown in Figure 1K.

The fluorescent image of the beating MMCs and EMCs was monitored using a CCD camera (Ikegami Tsushin Co., Ltd, http://www.ikegami.co.jp) and was stored using digital video. The video images (National Television Standards Committee format, 29.97 frame/second) of contraction of EMCs and MMCs were stored in a personal computer as MPEG-2 format files, then analyzed later.

Both edges of the EGFP-positive EMCs and MMCs along the line (Figs. 1L, 3K) were automatically detected, and the distance between both edges was measured from each video frame using an image edge-detection program using Igor Pro 4 (Wavemetrics Inc., Lake Oswego, OR) [11].

Calculation of Induction Rate

The MMCs and EMCs were exposed to 3 μM 5-azacytidine (5-azaC; Sigma-Aldrich) for 24 hours to induce cell differentiation, or were left untreated. The 5-azaC-treated and nontreated MMCs or EMCs, cultivated with or without murine fetal cardiomyocytes, were enzymatically dissociated and stained, then observed by confocal laser microscope (supplemental online data 2 for detail of method). The cardiomyogenic induction rate (average of 10 separate experiments) was calculated as the fraction of cardiac troponin-I-positive cells in the EGFP-positive cells.

Examination of Chromosomes of MMCs or EMCs and Murine Cell Chimeras

To rule out cell fusion-dependent cardiomyogenesis, chromosomes from MMCs or EMCs cocultivated without separation by the athelocollagen membrane from murine cardiomyocytes for 1 week were stained using a human chromosome-specific probe and a mouse chromosome-specific probe (Chromosome Science Labo, Hokkaido, Japan, http://www.chromoscience.jp/en/probe/page01/page01e.html) and spectral karyotyping with fluorescent in situ hybridization chromosome painting technique (Applied Spectral Imaging, Vista, CA, http://www.spectral-imaging.com), according to the manufacturer's protocol.

RNA Extraction and RT-PCR

Reverse transcriptase polymerase chain reaction (RT-PCR) was done as described previously [2]. Primers for the following genes were used: cardiac transcription factors—Csx/Nkx-2.5 and GATA4; cardiac hormones—atrial natriuretic peptide and brain natriuretic peptide; cardiac structural proteins—cardiac troponin I, cardiac troponin T, myosin light chain-2a, myosin light chain-2v, and cardiac-actin; and ion channel—cyclic nucleotide-gated potassium channel 2 (supplemental online Table 1). The internal control was 18S rRNA. PCR primers were prepared such that they would amplify the human but not the mouse genes.

Flow Cytometric Analysis

The cells were analyzed using an EPICS ALTRA analyzer (Beckman Coulter, Fullerton, CA, http://www.beckmancoulter.com). Antibodies (anti-human CD10, CD13, CD14, CD24, CD29, CD31, CD34, CD44, CD45, CD54, CD55, CD59, CD71, CD73, CDw90, CD105, CD106, CD117, CD133, CD140a, CD166, CD309, HLA-ABC, and HLA-DR) [12] were purchased from Beckman Coulter, Immunotech (Luminy, France, http://www.beckmancoulter.com/products/pr_immunology.asp), Cytotech (Hellebaek, Denmark, http://www.cytotech.dk/index.html), Santa Cruz Biotechnology Inc. (Santa Cruz, CA, http://www.scbt.com), RDI (Research Diagnostics, Inc., Concord, MA, http://www.researchd.com), and Pharmingen Pharmaceutical, Inc. (San Diego, http://www.bdbiosciences.com/index_us.shtml).

In Vivo Cardiomyogenic Differentiation of EMCs

EGFP-labeled EMC tissue graft, made by a novel 3-dimensional cell sheet manipulation, was transplanted into male F344 nude rats (Clea, Tokyo, http://www.clea-japan.com/) (8 weeks of age). EMC100s and EMC214s (2×10^5/cm^2) were plated onto fibrin polymer-coated culture dishes. Four days after plating, EMCs were detached as previously described [18], and transplanted onto the surface of the recipient heart (Fig. 5A) [19]. At 2 weeks after transplantation, immunohistochemical analysis was performed. EGFP-labeled EMC tissue graft on the fibrin polymer-coated culture dish did not show cardiomyogenic differentiation in vitro.

MMC Transplantation in Myocardial Infarction Model In Vivo

Recipient male F344 nude rats (Clea) (6 weeks of age) were anesthetized with 2% isoflurane gas. After left thoracotomy, the left ventricle was exposed and left anterior coronary artery was ligated by 6–0 silk suture. The complete occlusion of the coronary artery was confirmed by the cyanotic color and dyskinetic motion of the left ventricular anterior wall. In some rats, we did not ligate the coronary artery (Sham). The chest was closed and animals survived for 2 weeks to create complete myocardial infarction.

Two weeks after the first operation, rats with myocardial infarction were randomized for the control myocardial infarction (MI) group, the MI+BMMSC group, and the MI+MMC group, and were blinded immediately before the cell injection. Echocardiograms were performed on the anesthetized (2% isoflurane) rats. Data were collected three times and averaged. Immediately before transplantation, ~1–2 × 10^6 of EGFP-positive MMC or BMMSC suspension was drawn up into a 50-μl Hamilton syringe (Hamilton Co., Reno, NV, http://www.hamiltoncompany.com/main_usa.asp) with a 31-gauge needle. A 10-μl portion of the cell suspension was injected into the center and margin of the infarcted myocardium (MI+MMC, Fig. 7A). In the control MI group, culture medium or ~1–2 × 10^6 of murine cardiac fibroblast was injected. Immediately before cell transplantation, 2-dimensional and M-mode echocardiogmphic (8.5 MHz linear transducer, EnVisor C; Phillips Medical System, Andover, MA, http://www.medical.philips.com/index.html) images were obtained to assess left ventricular (LV) end-diastolic dimension and LV end-systolic dimension at the mid-papillary muscle level.

Two weeks after the transplantation, a similar echocardiogram was performed again; then after opening the abdomen, a blood sample was drawn from the abdominal great vein; then the left diaphragm was dissected to insert a 22-gauge manometer line into the left ventricle, which was connected to the transducer (model TP-400T; Nihon Kohden) to monitor left ventricular pressure. The electrocardiogram and measured pressure were digitized by PowerLabo (ADInstruments, Milford, MA, http://www.adinstruments.com) at the sample frequency of 10 KHz and stored in a personal computer (Macintosh iBook G4; Apple, Cupertino, CA, http://www.apple.com).

Tissue samples were obtained by fixing and slicing along the short axis of the left ventricle, for every 1-mm depth of the ventricle. After Masson's trichrome staining, digital images of samples were collected using a light microscope (IX-70; Olympus). The images were digitized and analyzed using an Igor Pro 4 (Wavemetrics Inc.). The pixel area of blue color (fibrosis area) was defined as the infarcted area, and the pixel area of red color was defined as "survived" myocardium. The data on each pixel area from each slice were collated and the percentage fibrosis area was calculated as follows: % Fibrosis = 100 × (Pixel area of blue color)/(Pixel area of blue color and red color).

Statistical Analysis

All data are shown as the mean value ± SE. The difference among mean values was determined with analysis of variance. The posthoc test (Bonferroni) was used when three or more groups were compared. Student's t test was used when two values were compared. Statistical significance was set at $p < .05$.

RESULTS

Cardiomyogenic Transdifferentiation of MMCs

To exclude cell fusion-dependent cardiomyogenesis [20], EGFP-labeled MMCs were cocultured in the same dish with mouse cardiomyocytes, separated by a 40-μm high-density athelocollagen membrane (Fig. 1M). The two cell types were never in direct contact. On day 5 after cocultivation commenced, approximately half of the MMCs were beating strongly in a synchronized manner (supplemental online Video 1). Im-

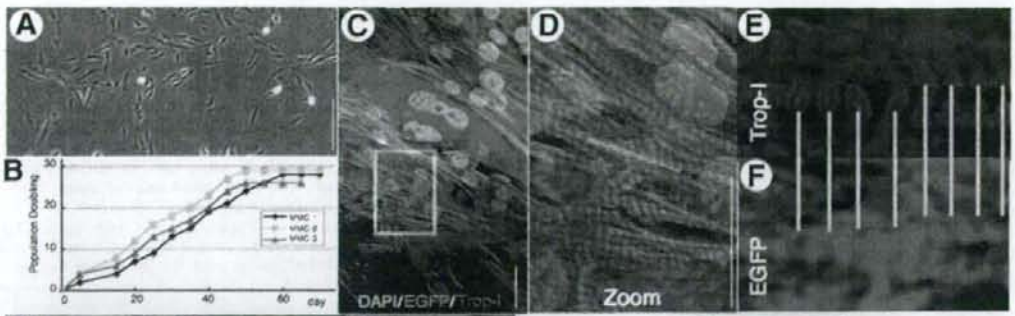

J

K

	MMC	EMC100	EMC214
APD90 (ms)	212 ± 28	326 ± 12	185 ± 16
MDP (mV)	-46 ± 3	-55 ± 1	-48 ± 3
Amplitude (mV)	48 ± 3	56 ± 7	56 ± 3
BCL (s)	0.69 ± 0.1	0.9 ± 0.1	2.4 ± 0.2
Pacemaker (+)	16/16	1/28	29/41

mean ± SE

Figure 1. Cardiomyogenic differentiation of menstrual blood-derived mesenchymal cells (MMCs) in vitro. **(A):** Phase-contrast microscopic view of MMC (bar denotes 100 μm), regarded as being PD1, or day 2. **(B):** The representative growth curves of MMCs as a function of time after the culture. The growth curves from all three donors are linear over at least 25 population doublings. **(C–F):** Laser confocal microscopic view of immunocytochemistry of differentiated MMCs with anti-cardiac troponin-I (Trop-I) antibody. Enhanced green fluorescent protein (EGFP)-positive (green) human MMCs expressed Trop-I (red). Scale bar denotes 20 μm. **(D):** Expansion of area within the white box in **(C)**. Clear striation pattern of Trop-I is observed. Trop-I and EGFP images along the yellow line are shown in **(E, F)**. **(E, F):** Trop-I and EGFP staining was observed alternately in striated manner, suggesting Trop-I is expressed in the EGFP-positive cell. **(G–I):** EGFP-labeled MMCs were injected with Alexa 568 solution (red) through a microelectrode to confirm that the recorded signal was obtained from MMCs. **(J):** Representative action potential traces are shown (horizontal line denotes 500 ms). The vertical line denotes 50 mV, and dotted horizontal line denotes 0 mV. **(K):** Action potential parameters. **(L):** A representative still image (left panel) and detected fractional shortening (% FS) along the white line obtained from sites a, b, and c are shown in right panel. **(M):** Experimental schema. Abbreviations: ADP, action potential duration; BCL, basic cycle length; DAPI, 4'-6-diamidino-2-phenylindole; MDP, maximum diastolic potential.

munocytochemistry revealed that the MMCs were stained positive by the anti-cardiac troponin-I antibody (Fig. 1C–1E). Clear striations of red fluorescence of troponin-I in the differentiated MMCs (Fig. 1D, 1E) were observed. Troponin-I and EGFP staining appeared alternately in a striated manner, suggesting troponin-I expressed in the EGFP-positive cell (Fig. 1E, 1F). Clear striations were observed with red fluorescence of α-actinin in the differentiated MMCs (Fig. 2B) and diffuse dot-like staining pattern of connexin 43 around the margin of each EGFP-positive cardiomyocyte (Fig. 2C–2F), suggesting that these human transdifferentiated cardiomyocytes have tight electrical coupling with each other. APs were recorded from spontaneously beating MMCs. The APs obtained from MMCs showed clear cardiomyocyte-specific sustained plateaus and slowly depolarizing resting membrane potentials—so-called "pacemaker potentials" (Fig. 1J, 1K)—and were, therefore, determined to be APs of cardiomyocytes, not of smooth muscle cells, nerve cells, or skeletal muscle cells. The fractional shortening (% FS) of the MMCs was analyzed (Fig. 1L) using a cell edge detection program. The EGFP-positive cells contracted simultaneously within the whole visual field. The % FS was 5.9 ± 0.5% (n = 19).

The percentage of cardiac troponin-I-positive cells was calculated to determine the cardiomyogenic transdifferentiation rate. Whereas MMCs without cocultivation did not show any troponin-I expression (supplemental online Figs. 1A–1D, 2A, 2B), 27%–32% of MMCs became positive for cardiac troponin-I antibody as a result of the cocultivation (Figs. 1C–1F, 4A, supplemental online Fig. 2C, 2D). A cytosine analog, 5-azaC, has a remarkable effect on cell transdifferentiation and has been shown to induce transdifferentiation BMMSCs into cardiomyocytes in mice by nonspecific demethylation of the genome [1]. Cardiomyogenic transdifferentiation was observed in the cocultivated MMCs without any 5-azaC pretreatment, meaning that 5-azaC was not essential for cardiomyogenic transdifferentiation. Nuclear fusion between the cocultivated MMCs and murine cardiomyocytes without separation of the athelocollagen membrane was observed in only 0.16% (3/1846).

Cardiomyogenic Transdifferentiation of EMCs

We hypothesized that the origin of cardiomyogenic cells in the MMCs was the endometrial gland, since MMCs have a high content of detached endometrial glands, whereas circu-

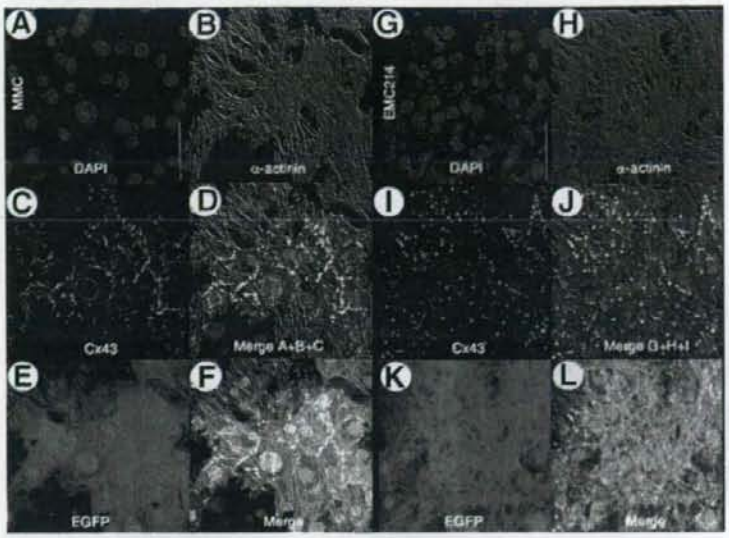

Figure 2. Immunocytochemical analysis of menstrual blood-derived mesenchymal cells (MMCs) and EMC214s stained with anti-sarcomeric α-actinin and connexin 43. **(A–L):** Laser confocal microscopic view of immunocytochemistry of differentiated MMCs and EMC214s with anti-sarcomeric α-actinin (α-actinin) and connexin 43 (Cx43) antibody. **(A–F, G–L):** Enhanced green fluorescent protein (EGFP)-positive **(E, K;** green) human MMCs and EMC214s express α-actinin **(B, H;** red) and Cx43 **(C, I;** cyan). Nuclei are stained with 4′-6-diamidino-2-phenylindole (DAPI) **(A, G;** blue). Clear striation patterns of α-actinin and diffuse Cx43 dot-like staining around the margin of the MMCs and EMC214s were observed. Scale bars in the figure denote 50 μm.

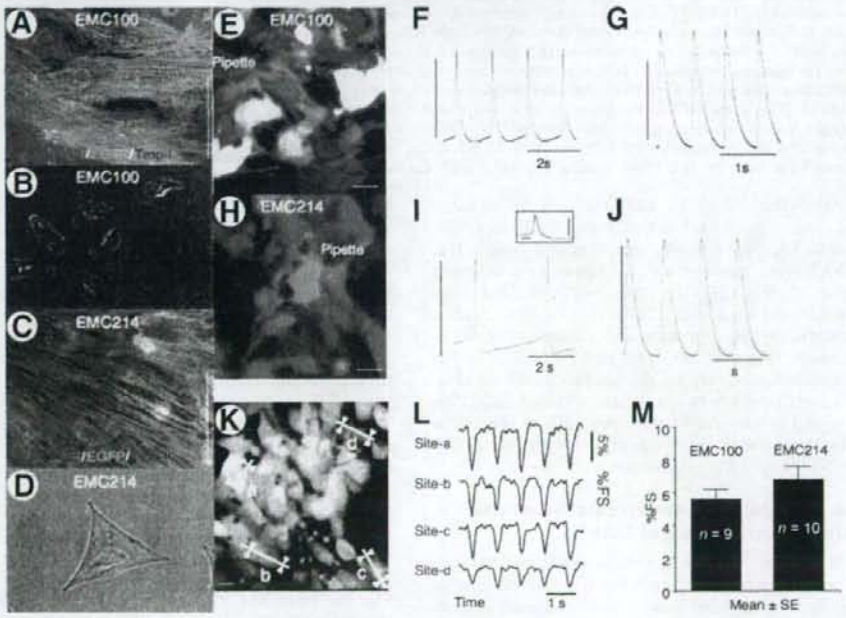

Figure 3. Cardiomyogenic differentiation of endometrial gland-derived mesenchymal cells (EMCs) in vitro. **(A, C):** Immunocytochemistry of differentiated EMC100s **(A)** and EMC214s **(C)** with anti-cardiac troponin-I (Trop-I) antibody. The cells were stained with 4′-6-diamidino-2-phenylindole (DAPI; blue), and anti-cardiac troponin-I antibody (red). Enhanced green fluorescent protein (EGFP)-positive (green) human EMCs expressed Trop-I (red). Please note clear striation staining pattern of Trop-I **(A, C)** in EMCs. Scale bar denotes 20 μm. **(B, D):** Phase-contrast images of EMC100s **(B)** and EMC214s **(D)** before the cardiomyogenic induction. **(E, H):** EGFP-labeled EMC100s and EMC214s (green) were injected with Alexa 568 solution (red) through a microelectrode **(E, H)**, and a recorded signal was obtained from the cells. Representative action potential traces are shown **(F, G:** EMC100; **I, J:** EMC214). Action potential of E is expanded in the inset (the vertical line denotes 100 ms). The vertical line denotes 50 mV and dotted horizontal line denotes 0 mV levels. **(K–M):** A representative still image **(K)** and detected fractional shortening (% FS) along the white line obtained from sites a, b, c, and d in **(L)** are shown in **(M)**. **(M):** The measured % FS was averaged and is shown.

lating blood-derived endothelial progenitor cells [21] or marrow-derived MSCs [2] do not have such high cardiomyogenic differentiation ability. We consequently established a line of EMCs (Fig. 3B, 3D) with a lifespan prolonged by a cell cycle-mediated gene to ensure a supply of cells for analysis. Almost all EMCs beat strongly in a synchronized manner

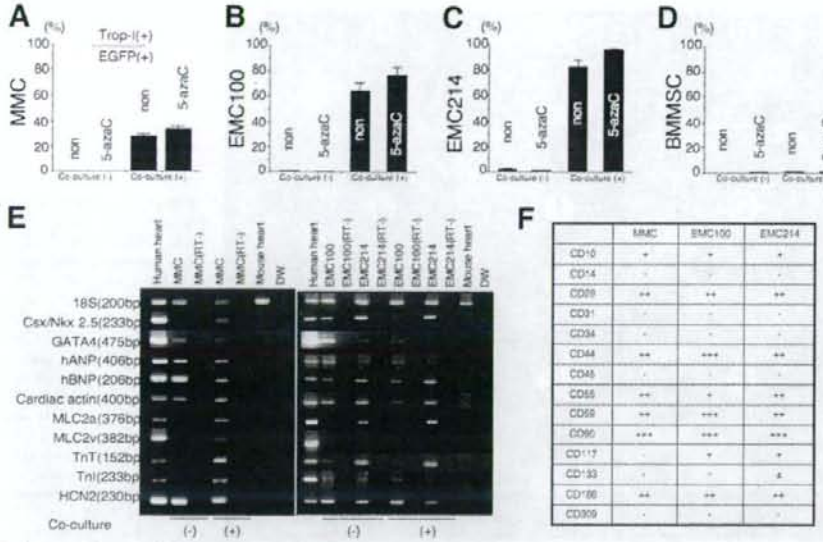

	MMC	EMC100	EMC214
CD10	+	+	+
CD14	-	-	-
CD29	++	++	++
CD31	-	-	-
CD34	-	-	-
CD44	++	+++	++
CD45	-	-	-
CD55	++	+	++
CD59	++	+++	++
CD90	+++	+++	+++
CD117	-	+	+
CD133	-	-	±
CD166	++	++	++
CD309	-	-	-

Figure 4. Cardiomyogenic transdifferentiation rates and expression of cardiomyocyte-specific genes and cell surface markers of menstrual blood-derived mesenchymal cells (MMCs) and endometrial gland-derived mesenchymal cells (EMCs). **(A–D):** Cardiomyogenic transdifferentiation rates of MMCs, EMCs, and bone marrow-derived mesenchymal stem cells (BMMSCs). The character in each column denotes pretreatment with 5-azacytidine (5-azaC) or the lack of treatment (non). **(E):** Reverse transcriptase polymerase chain reaction (PCR) was performed with PCR primers with specificity for human genes encoding cardiac proteins but not for the corresponding murine genes (supplemental online Table 1). Human heart and mouse heart cells were used as a positive control and negative control, respectively. Most human cardiac genes were constitutively expressed in the default state of MMCs and EMCs. **(F):** Summary of flow cytometric analysis of MMCs and EMCs with fluorescein isothiocyanate–coupled antibodies against human surface antigens. Abbreviations: DW, distilled water; EGFP, enhanced green fluorescent protein; hANP, human atrial natriuretic peptide; hBNP, human brain natriuretic peptide; HCN2, cyclic nucleotide-gated potassium channel 2; MLC2a, myosin light chain 2a; MLC2V, myosin light chain 2v; TnI, Trop-I, cardiac troponin I; TnT, cardiac troponin T.

(supplemental online Video 1), and 76.4%–96.5% became positive for cardiac troponin-I antibody as a result of cocultivation (Figs. 3A, 3C, 4B, 4C, supplemental online Fig. 2E–2L). EMCs were also positive for sarcomeric α-actinin and connexin 43 (Fig. 2G–2L). APs were recorded from EMCs. The APs obtained from EMCs showed clear cardiomyocyte-specific sustained plateaus and, in some cells, pacemaker potentials (Fig. 3E–3J). The EGFP-positive EMCs contracted simultaneously within the whole visual field (Fig. 3L, 3M). Nuclear fusion between the cocultivated EMC100s or EMC214s and murine cardiomyocytes without separation of the athelocollagen membrane was observed in only 0.57% (6/1058) or 0.28% (5/1758), respectively.

Expression of Cardiomyocyte-Specific Genes and Surface Markers of EMCs and MMCs

The RT-PCR was performed with primers that hybridized with human cardiomyocyte-specific genes but not with the murine orthologs. Differentiated MMCs and EMCs expressed cardiac-specific genes (Fig. 4D). Interestingly, most of the analyzed genes were expressed in the cells before the induction of transdifferentiation by cocultivation.

There is no difference between surface markers of the MMCs and EMCs. Both cells were positive for CD29 (integrin β1), CD59, and negative for CD14, CD34, CD45, CD309 (Flk-1), etc. (Fig. 4E, supplemental online Fig. 3A–3C).

Cardiomyogenic Effects In Vivo

An EGFP-labeled EMC tissue graft made by a novel 3-dimensional cell sheet manipulation [18] was transplanted into male F344 nude rats to ensure in vivo cardiomyogenic transdifferentiation ability. The EGFP-positive cell layer (green) was observed at the epicardial surface of the host heart (Fig. 5B–5D). Whole EMCs throughout the layer expressed a clear striation staining pattern of sarcomeric α-actinin (Fig. 5B–5G), suggesting extremely high cardiomyogenic transdifferentiation ability of EMCs in situ.

MMCs or BMMSCs were transplanted into the nude rats with MI in vivo. Echocardiography showed that the left ventricular fractional shortening (% LVFS) in the MI+MMC group was significantly greater than it in the MI+BMMSC group at 2 weeks after transplantation (Fig. 6A–6I, supplemental online Fig. 4). The MI area was digitized and every 1-mm depth of tissue section stained with Masson's trichrome (Fig. 6J–6O); averaged data are shown in Figure 6P. The MI area was significantly lower in the MI+MMC group than in the MI+BMMSC group. The EGFP-positive mass of MMCs observed in the MI area expressed a clear striation staining pattern of cardiac troponin-I (Fig. 7) and sarcomeric α-actinin (supplemental online Fig. 5), suggesting an extremely high in situ cardiomyogenic transdifferentiation ability of MMCs, which contributed to improvement in cardiac function.

Discussion

Mechanisms of Highly Cardiomyogenic Transdifferentiation Ability of MMCs and EMCs

The gene expression pattern of MMCs and EMCs before cardiomyogenic transdifferentiation is quite different from that of marrow-derived MSCs [2]. GATA-4 expression in the MMCs and EMCs, and Csx/Nkx 2.5 expression in EMCs with the

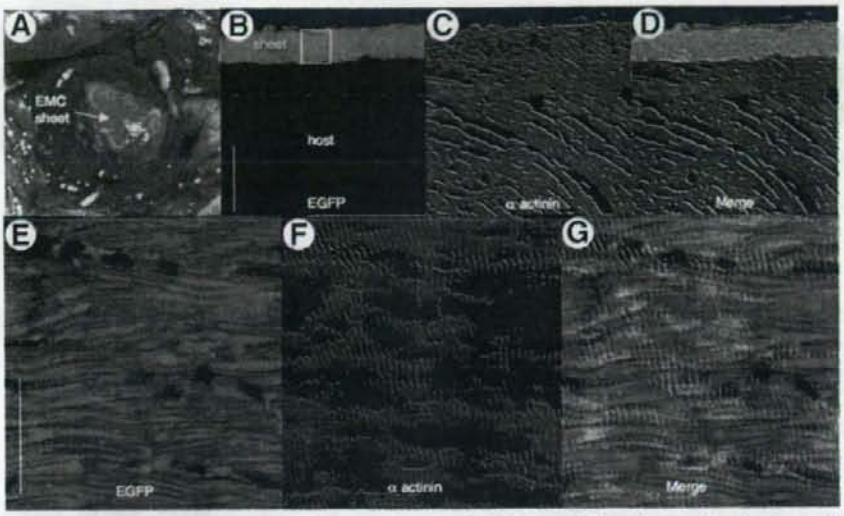

Figure 5. In vivo cardiomyogenesis of endometrium-derived mesenchymal cells (EMCs) in cell sheet tissue graft on host heart. **(A):** Macroscopic view of enhanced green fluorescent protein (EGFP)-labeled EMC tissue graft (sheet) on the epicardial surface of the recipient's heart. **(B–D):** Two weeks after transplantation, immunohistochemistry revealed survival of EMC tissue layer (green) on the recipient heart. Scale bar denotes 100 μm. **(C):** Engrafted EMCs stained positive with anti-sarcomeric α-actinin (red; α-actinin). **(E–G):** The area in the white box in **(B)** is shown in greater detail in **(E–G)**. **(F):** The clear striation pattern of α-actinin staining was observed throughout the entire layer of engrafted EMCs, suggesting extremely high cardiomyogenic potential of EMCs in situ. Scale bar denotes 20 μm.

ability of self-renewal suggest that MMCs and EMCs both have cardiogenic potential and may be termed "cardiac precursor cells" due to their biological features. Cardiac mRNA but not cardiac protein (i.e., troponin-I) was expressed at the default state in the present study, suggesting that both genetic and epigenetic factors may be essential to cause physiologically functioning cardiomyogenic differentiation in MMCs and EMCs. The mechanism of the drastic improvement in the transdifferentiation rate of MMCs and EMCs may be attributable to the default characteristics (expression level of cardiomyocyte-specific mRNA) of MMCs and EMCs in culture compared to marrow-derived MSCs. Highest cardiomyogenic transdifferentiation efficiency was observed in EMC214s (96.5%), EMC100s (76.4%), UCBMSCs (44.9%) [11], MMCs (33.2%), PCPCs (15.1%) [12], and BMMSCs (0.3%, Fig. 4D) [2] in that order. In the practical point of view, EMCs and UCBMSCs are difficult to obtain in enough numbers during the first few passages. MMCs are, therefore, the most suitable cellular source for cardiac stem cell therapy, having a high cardiomyogenic transdifferentiation efficiency. MMCs, EMCs, UCBMSC, and PCPCs are derived from the organ that is related to the pregnancy, therefore the high cardiomyogenic transdifferentiation ability of mesenchymal cells may be caused by a pregnancy-related environmental condition.

Origin of the MMCs and EMCs

Cell surface marker analysis revealed that MMCs are neither encirculating endothelial progenitor cells [22] nor macrophages, but are mesenchymal phenotype cells. We speculated that MMCs may originate in uterine endometrial glands since a lot of detached endometrial glands were observed in menstrual blood and EMCs have the same surface marker as the MMCs, as well as an extremely high cardiomyogenic potential (76.4%–96.5% and 33.2%, respectively). As has been reported, MSCs cannot be detected in circulating blood and all tissues have MSC reservoirs localized in the perivascular niche [23], so EMCs and MMCs do not seem to originate from BMMSCs.

Clinical Contribution

In the present study, MMC transplantation improved impaired cardiac function in vivo. Since MMCs were transplanted at 2 weeks after coronary occlusion, when myocardial necrosis had been completed, the improvement of cardiac function is not due only to transplanted MMC-induced neovascularization [7, 8] or an antiapoptotic [9] effect on infarcted cardiomyocytes. Since they display high cardiomyogenic transdifferentiation ability in vitro and massive cardiomyogenic transdifferentiation in vivo, MMC-derived cardiomyocytes may play a role in the improvement of cardiac function in the present study. Myocardial infarction is known to suppress contraction ability of cardiomyocytes even at normal zone by left ventricular remodeling. Therefore MMC-derived paracrine factors may also play an important role in recovery of % LVFS by prevention of development of LV remodeling.

Neovascularization and the antiapoptotic effect are important for improving cardiac function to some extent. However, the feasible effect is dependent on the number of residual host cardiomyocytes in the infarcted myocardium. To achieve further improvement of cardiac function, a stem cell source that can be expected to exhibit powerful cardiomyogenic transdifferentiation in situ is required. MMCs can be transdifferentiated into cardiomyocytes in situ on the recipient heart, suggesting that they are a promising source for cardiac stem cell-based therapy material, significantly more efficient for cardiomyogenesis than BMMSCs.

MMCs can be readily obtained in a noninvasive manner from young female volunteers, and stored. It should therefore be possible to obtain MMCs of all the HLA types, possibly enabling the establishment of an MMC bank system to facilitate cardiac stem cell-based therapy.

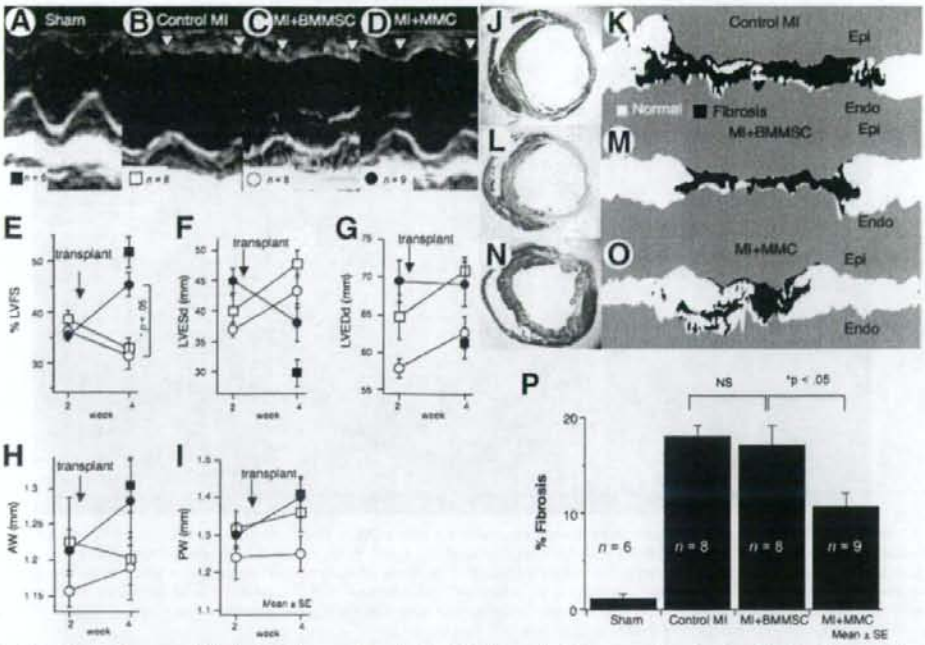

Figure 6. The effect of menstrual blood-derived mesenchymal cell (MMC) transplantation on cardiac function. **(A–D):** Representative M-mode echocardiographic images. The contraction of the left ventricular (LV) anterior wall was improved by transplantation of MMCs (white arrows). The symbol of and number in each group is depicted at the bottom left of each image. **(E–I):** Measured LV parameters are averaged and shown at 2 weeks and 4 weeks after the myocardial infarction (MI). The significant improvement of **(F)** LV end-systolic diameter (LVESd) and **(E)** % fractional shortening (% LVFS) were observed. The diameter of **(H)** anterior left ventricular wall thickness (AW), and **(I)** posterior left ventricular wall thickness (PW). There is no statistical significance. **(J–O):** Representative Masson's trichrome stain images **(J, L, N)** and digitized images **(K, M, O)** of control MI group, MI+bone marrow-derived mesenchymal stem cell (BMMSC), and MI+MMC group are shown. **(P):** The calculated % fibrosis areas are summed and averaged. The MMC transplantation showed significant reduction of % fibrosis area. Abbreviations: Endo, endocardium; Epi, epicardium; NS, not significant.

Role of Established Cardiomyogenic EMC Cell Line for Determining Cardiomyogenic Factors

Several stem cell types are used for clinical patients. Of these, MSCs are reported to show cardiomyogenesis in vitro. Thus, the analysis of key mechanisms for cardiomyogenic differentiation in the human mesenchymal cell is extremely important in order to expand the efficacy of current cardiac stem cell therapy. However, it is very difficult to specify the key factor of cardiomyogenesis by in vivo experiment only. Establishment of EMCs and an in vitro cardiomyogenic differentiation assay system are essential. Stable and high cardiomyogenic transdifferentiation ability in our established system enables us to observe, with wide dynamic range, the effects of treatment for cardiomyogenesis. Moreover, the primary culture condition of murine cardiomyocytes usually fluctuates due to variations in environments, the skill of individual researchers, and institutional differences in isolation protocols. Our established EMCs may provide a good positive control for a cardiomyogenic assay system in vitro to check whether the feeder cell condition is suitable for cardiomyogenic assay. When feeder conditions are suitable, we can survey for possible cardiomyogenic assistant factors or appropriate culture conditions for human BMMSCs by applying various agents or modifying culture conditions systematically. Thus, by using our EMCs and cocultivation system, we may be able to expand the cardiomyogenic differentiation potential of marrow-derived MSCs. Consequently, we may be able to increase the efficacy of cardiac stem cell-based therapy dramatically.

Neither passive stretching of EMCs nor an application of the supernatant of murine cardiomyocyte culture medium to the EMCs alone caused cardiomyocyte differentiation. Taking these findings into account, the multiple environmental factors, including mechanical stretching and/or feeder cardiomyocyte-derived humoral factors, seem to contribute to cardiomyogenic transdifferentiation in human mesenchymal cells. Further experiments should be done.

Study Limitations

Cell fusion between the human cells (MMCs or EMCs) might be a major cause of EGFP-positive cardiomyocytes in the present study. However, EGFP-positive cardiomyocytes could be observed, even when human cells and murine cardiomyocytes were cocultured separately by the athelocollagen membrane that is permeable for only small molecules (less than 5,000 MW)—thus allowing no possible penetration of cells or organelles through the membrane (supplemental online Fig. 6). Furthermore, even if the cells were cocultured without the athelocollagen membrane, nuclear fusion between EMC100s, EMC214s, or MMCs and fetal murine cardiomyocytes was less than 1% in the present study. Moreover, transdifferentiated EMCs at the external layer of the cell sheet graft on the epicardial surface did not directly contact the host cardiomyocytes (Fig. 5). Taking these results

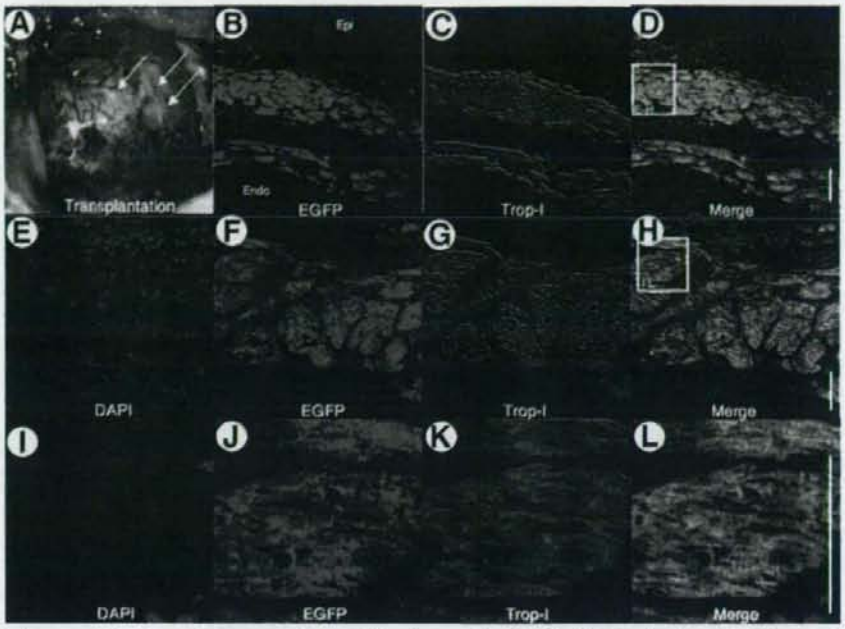

Figure 7. Cardiomyogenesis of engrafted menstrual blood-derived mesenchymal cells (MMCs) in vivo. **(A):** Macroscopic view of the recipient's heart immediately after enhanced green fluorescent protein (EGFP)-labeled MMC transplantation (white arrows) into the myocardial infarction area of the recipient's heart. **(B–L):** Two weeks after transplantation, immunohistochemistry revealed survival of the MMC tissue layer (green) on the treated heart. **(B–D):** Engrafted MMCs stained positive with anti-cardiac troponin-I (red; Trop-1). Scale bar denotes 100 μm. **(E–H, I–L):** The area in the white box in **(D)** was observed in higher resolution **(E–H)** and the white box in **(H)** was also observed in higher resolution **(I–L). (K):** The clear striation pattern of Trop-1 staining was observed throughout the whole layer of engrafted MMCs, suggesting extremely high cardiomyogenic potential of MMCs in situ. Scale bar denotes 20 μm. Abbreviations: DAPI, 4′-6-diamidino-2-phenylindole; Endo, endocardium; Epi, epicardium.

into account, we concluded that the cell fusion did not play a major role in the observed significant cardiomyogenic potential of MMCs and EMCs in the present study.

Infarcted heart tissue may increase auto-fluorescence in some fixative conditions and such auto-fluorescence of host cardiomyocytes might be confused as EGFP-positive like cells. However, autofluorescence of the host myocardium adjacent to the infarcted area was not significant in our present condition (Figs. 5B, 6B, supplemental online Fig. 5B, 5F). Therefore, EGFP-positive tissue in the present study can be defined as of human cell origin and easily distinguished from the host heart by the EGFP fluorescent intensity.

The transfection of the cell cycle-mediated gene may increase cardiomyogenic differentiation to some extent. However, our previous study in human BMMSCs, [2] with the same combination of cell cycle-mediated gene transfection, did not show any increase in efficiency. Furthermore, non-gene-transfected MMCs have an extremely high cardiomyogenic efficiency compared to gene-transfected BMMSCs. Taking these results into account, we concluded that transfection of those genes does not play an essential role in causing such high cardiomyogenic differentiation efficiency in EMCs.

In comparison to previous papers, there was no observable effect of BMMSC transplantation on cardiac function in the present study. This discrepancy may be caused by different experimental conditions, that is, species difference between BMMSCs and the host animal [24], transplantation at acute myocardial infarction [25–27], and usage of immunosuppressive agents, etc [24–27].

In the present study, we did not use a pressure-tipped catheter, therefore the LV dp/dt value may be underestimated.

Summary

MMC transplantation decreased fibrosis area and restored the LV systolic function in the MI-model in vivo. Engrafted MMC transdifferentiated into cardiomyocyte within MI area. MMC can be a major cell source for stem cell therapy to achieve cardiomyogenesis.

Acknowledgments

The research of N.H. and N.N. was partially supported by a grant from the Ministry of Education, Science and Culture, Japan. A part of this work was undertaken at the Keio Integrated Medical Research Center. We thank M. Uchiyama, A. Furuta, K. Hayakawa, and K. Okamoto for help during the experiments. N.H. and N.N. contributed equally to this work. A part of this work was reported at the annual meeting of the American College of Cardiology 2005, 2006, and 2007.

Disclosure of Potential Conflicts of Interest

The authors indicate no potential conflicts of interest.

REFERENCES

1 Makino S, Fukuda K, Miyoshi S et al. Cardiomyocytes can be generated from marrow stromal cells in vitro. J Clin Invest 1999;103:697–705.
2 Takeda Y, Mori T, Imabayashi H et al. Can the life span of human marrow stromal cells be prolonged by bmi-1, E6, E7, and/or telomerase without affecting cardiomyogenic differentiation? J Gene Med 2004;6: 833–845.
3 Chen SL, Fang WW, Ye F et al. Effect on left ventricular function of intracoronary transplantation of autologous bone marrow mesenchymal stem cell in patients with acute myocardial infarction. Am J Cardiol 2004;94:92–95.
4 Orlic D, Kajstura J, Chimenti S et al. Bone marrow cells regenerate infarcted myocardium. Nature 2001;410:701–705.
5 Wang JS, Shum-Tim D, Galipeau J et al. Marrow stromal cells for cellular cardiomyoplasty: Feasibility and potential clinical advantages. J Thorac Cardiovasc Surg 2000;120:999–1005.
6 Shake JG, Gruber PJ, Baumgartner WA et al. Mesenchymal stem cell implantation in a swine myocardial infarct model: Engraftment and functional effects. Ann Thorac Surg 2002;73:1919–1926.
7 Gojo S, Gojo N, Takeda Y et al. In vivo cardiovasculogenesis by direct injection of isolated adult mesenchymal stem cells. Exp Cell Res 2003; 288:51–59.
8 Tang YL, Zhao Q, Zhang YC et al. Autologous mesenchymal stem cell transplantation induce VEGF and neovascularization in ischemic myocardium. Regul Pept 2004;117:3–10.
9 Gnecchi M, He H, Liang O et al. Paracrine action accounts for marked protection of ischemic heart by Akt-modified mesenchymal stem cells. Nat Med 2005;11:367–368.
10 Kocher AA, Schuster MD, Szabolcs MJ et al. Neovascularization of ischemic myocardium by human bone-marrow-derived angioblasts prevents cardiomyocyte apoptosis, reduces remodeling and improves cardiac function. Nat Med 2001;7:430–436.
11 Nishiyama N, Miyoshi S, Hida N et al. The significant cardiomyogenic potential of human umbilical cord blood-derived mesenchymal stem cells in vitro. STEM CELLS 2007;25:2017–2024.
12 Okamoto K, Miyoshi S, Toyoda M et al. 'Working' cardiomyocytes exhibiting plateau action potentials from human placenta-derived extraembryonic mesodermal cells. Exp Cell Res 2007;313:2550–2562.
13 Terai M, Uyama T, Sugiki T et al. Immortalization of human fetal cells: the life span of umbilical cord blood-derived cells can be prolonged without manipulating p16INK4a/RB braking pathway. Mol Biol Cell 2005;16:1491–1499.
14 Takeuchi M, Takeuchi K, Kohara A et al. Chromosomal instability in human mesenchymal stem cells immortalized with human papilloma virus E6, E7, and Htert genes. In Vitro Cell Dev Biol Anim 2007;43: 129–138.
15 Schwab KE, Gargett CE. Co-expression of two perivascular cell markers isolates mesenchymal stem-like cells from human endometrium. Hum Reprod 2007;22:2903–2911.
16 Meng X, Ichim TE, Zhong J et al. Endometrial regenerative cells: A novel stem cell population. J Transl Med 2007;5:57–66.
17 Kyo S, Nakamura M, Kiyono T et al. Successful immortalization of endometrial glandular cells with normal structural and functional characteristics. Am J Pathol 2003;163:2259–2269.
18 Itabashi Y, Miyoshi S, Kawaguchi H et al. A new method for manufacturing cardiac cell sheets using fibrin-coated dishes and its electrophysiological studies by optical mapping. Artificial Organs 2004;29:95–103.
19 Furuta A, Miyoshi S, Itabashi Y et al. Pulsatile cardiac tissue grafts using a novel three-dimensional cell sheet manipulation technique functionally integrates with the host heart, in vivo. Circ Res 2006;98:705–712.
20 Iijima Y, Nagai T, Mizukami M et al. Beating is necessary for transdifferentiation of skeletal muscle-derived cells into cardiomyocytes. FASEB J 2003;17:1361–1363.
21 Koyanagi M, Urbich C, Chavakis E et al. Differentiation of circulating endothelial progenitor cells to a cardiomyogenic phenotype depends on E-cadherin. FEBS Lett 2005;579:6060–6066.
22 Asahara T, Murohara T, Sullivan A et al. Isolation of putative progenitor endothelial cells for angiogenesis. Science 1997;275:964–967.
23 da Silva Meirelles L, Chagastelles PC, Nardi NB. Mesenchymal stem cells reside in virtually all post-natal organs and tissues. J Cell Sci 2006;119:2204–2213.
24 Wang JA, Fan YQ, Li CL et al. Human bone marrow-derived mesenchymal stem cells transplanted into damaged rabbit heart to improve heart function. J Zhejiang Univ Sci B 2005;6:242–248.
25 Zhang S, Ge J, Sun A et al. Comparison of various kinds of bone marrow stem cells for the repair of infarcted myocardium: Single clonally purified non-hematopoietic mesenchymal stem cells serve as a superior source. J Cell Biochem 2006;99:1132–1147.
26 Grauss RW, Winter EM, van Tuyn J et al. Mesenchymal stem cells from ischemic heart disease patients improve left ventricular function after acute myocardial infarction. Am J Physiol Heart Circ Physiol 2007;293: H2438–H2447.
27 Hou M, Yang KM, Zhang H et al. Transplantation of mesenchymal stem cells from human bone marrow improves damaged heart function in rats. Int J Cardiol 2007;115:220–228.

See www.StemCells.com for supplemental material available online.

Gremlin Enhances the Determined Path to Cardiomyogenesis

Daisuke Kami[1,3], Ichiro Shiojima[4], Hatsune Makino[1], Kenji Matsumoto[2], Yoriko Takahashi[1], Ryuga Ishii[1], Atsuhiko T. Naito[4], Masashi Toyoda[1], Hirohisa Saito[2], Masatoshi Watanabe[3], Issei Komuro[4], Akihiro Umezawa[1]*

1 Department of Reproductive Biology, National Institute for Child Health and Development, Tokyo, Japan, **2** Department of Allergy and Immunology, National Institute for Child Health and Development, Tokyo, Japan, **3** Laboratory for Medical Engineering, Division of Materials Science and Chemical Engineering, Graduate School of Engineering, Yokohama National University, Yokohama, Japan, **4** Department of Cardiovascular Science and Medicine, Chiba University Graduate School of Medicine, Chiba, Japan

Abstract

Background: The critical event in heart formation is commitment of mesodermal cells to a cardiomyogenic fate, and cardiac fate determination is regulated by a series of cytokines. Bone morphogenetic proteins (BMPs) and fibroblast growth factors have been shown to be involved in this process, however additional factors needs to be identified for the fate determination, especially at the early stage of cardiomyogenic development.

Methodology/Principal Findings: Global gene expression analysis using a series of human cells with a cardiomyogenic potential suggested *Gremlin* (*Grem1*) is a candidate gene responsible for *in vitro* cardiomyogenic differentiation. Grem1, a known BMP antagonist, enhanced DMSO-induced cardiomyogenesis of P19CL6 embryonal carcinoma cells (CL6 cells) 10–35 fold in an area of beating differentiated cardiomyocytes. The Grem1 action was most effective at the early differentiation stage when CL6 cells were destined to cardiomyogenesis, and was mediated through inhibition of BMP2. Furthermore, BMP2 inhibited Wnt/β-catenin signaling that promoted CL6 cardiomyogenesis.

Conclusions/Significance: Grem1 enhances the determined path to cardiomyogenesis in a stage-specific manner, and inhibition of the BMP signaling pathway is involved in initial determination of Grem1-promoted cardiomyogenesis. Our results shed new light on renewal of the cardiovascular system using Grem1 in human.

Citation: Kami D, Shiojima I, Makino H, Matsumoto K, Takahashi Y, et al. (2008) Gremlin Enhances the Determined Path to Cardiomyogenesis. PLoS ONE 3(6): e2407. doi:10.1371/journal.pone.0002407

Editor: Hernan Lopez-Schier, Centre de Regulacio Genomica, Spain

Received January 15, 2008; **Accepted** May 5, 2008; **Published** June 11, 2008

Funding: This study was supported by a grant from the Ministry of Education, Culture, Sports, Science and Technology (MEXT) of Japan and Health and Labor Sciences Research Grants; by a Research grant on Health Science Focusing on Drug Innovation from the Japan Health Science Foundation; by the Program for Promotion of Fundamental Studies in Health Science of the Pharmaceuticals and Medical Devices Agency; by a grant from the Terumo Life Science Foundation; by a Research Grant for Cardiovascular Disease from the Ministry of Health, Labor and Welfare (MHLW); and by a Grant for Child Health and Development from the MHLW.

Competing Interests: The authors have declared that no competing interests exist.

* E-mail: umezawa@1985.jukuin.keio.ac.jp

Introduction

The critical event in heart formation is commitment of mesodermal cells to a cardiomyogenic fate and their migration into anterolateral regions of the embryo during late gastrulation. In this process, morphogenic movements and cardiac fate determination are regulated by cytokines such as bone morphogenetic proteins (BMPs) [1–3], and fibroblast growth factors (FGFs) [4–7]. These secreted proteins from neighboring endoderm, ectoderm, and the mesoderm itself, play important roles in induction of cardiac transcription factors [8] and differentiation of cardiomyocytes in amphibians [9] and avians [4]. Cardiomyogenic signals, such as BMPs and FGFs, indeed activate expression of cardiac specific transcriptional factors (Csx/Nkx2.5, Gata4, Mef2c), and these transcriptional factors activate expression of circulating hormones (atrial natriuretic peptide (ANP), brain natriuretic peptide (BNP)), and cardiac specific proteins (myosin heavy chain (MyHC), myosin light chain (MyLC)). Wnt family proteins, cysteine-rich, and secreted glycoproteins, have also been implicated in embryonic development [10,11], and cardiomyogenesis [12,13]. In *Drosophila*, '*wingless*', a homologue of vertebrate Wnt is involved in expression of '*tinman*', a *Drosophila* homologue of Csx/Nkx2.5, through '*armadillo*', a *Drosophila* ortholog of β-catenin, and drives heart development [14]. In vertebrates, however, Wnt1/3a, which activates the canonical Wnt/β-catenin signaling pathway leading to stabilization of β-catenin as a downstream molecule through inactivation of glycogen synthase kinase-3β, inhibits cardiomyocytic differentiation from cardiac mesoderm [15–18]. Wnt11 promotes cardiac differentiation via the non-canonical pathway in *Xenopus* [12] and murine embryonic cell lines [19]. The secretion of Wnt inhibitors such as 'Cerberus', 'Dickkopf' and 'Crescent' by the anterior endoderm prevents Wnt3a secreted by the neural tube from inhibiting heart formation [15–17].

In this study, we performed GeneChip analysis to identify multiple extracellular determinants, such as cytokines, cell